

University of Alberta

**Fabrication and Testing of
Waveguides in Chalcogenide Glass**

by

Qingbin (Ben) Zheng



A thesis submitted to the Faculty of Graduate Studies and Research in partial fulfillment
of the requirements for the degree of Master of Science

Department of Electrical and Computer Engineering

Edmonton, Alberta

Spring 2004



Library and
Archives Canada

Bibliothèque et
Archives Canada

Published Heritage
Branch

Direction du
Patrimoine de l'édition

395 Wellington Street
Ottawa ON K1A 0N4
Canada

395, rue Wellington
Ottawa ON K1A 0N4
Canada

Your file *Votre référence*
ISBN: 0-612-96574-0
Our file *Notre référence*
ISBN: 0-612-96574-0

The author has granted a non-exclusive license allowing the Library and Archives Canada to reproduce, loan, distribute or sell copies of this thesis in microform, paper or electronic formats.

L'auteur a accordé une licence non exclusive permettant à la Bibliothèque et Archives Canada de reproduire, prêter, distribuer ou vendre des copies de cette thèse sous la forme de microfiche/film, de reproduction sur papier ou sur format électronique.

The author retains ownership of the copyright in this thesis. Neither the thesis nor substantial extracts from it may be printed or otherwise reproduced without the author's permission.

L'auteur conserve la propriété du droit d'auteur qui protège cette thèse. Ni la thèse ni des extraits substantiels de celle-ci ne doivent être imprimés ou autrement reproduits sans son autorisation.

In compliance with the Canadian Privacy Act some supporting forms may have been removed from this thesis.

Conformément à la loi canadienne sur la protection de la vie privée, quelques formulaires secondaires ont été enlevés de cette thèse.

While these forms may be included in the document page count, their removal does not represent any loss of content from the thesis.

Bien que ces formulaires aient inclus dans la pagination, il n'y aura aucun contenu manquant.

Canada

Abstract

Chalcogenide glasses have unique properties and are now getting increasing attention in the electronic and opto-electronic industries. Scientists are looking for ways to utilize them in the field of integrated optics. Waveguides, including straight waveguides, curved waveguides and Y-branches, form a basis for various applications of chalcogenide glasses. With strip-loaded shallow rib waveguides, relatively low coupling losses and propagation losses can be achieved in the infrared region for chalcogenide glasses while maintaining single-mode propagation.

In this project, single-mode chalcogenide strip-loaded shallow rib waveguides were designed and fabricated. First, simulations were undertaken using the effective index method, the finite difference method and the beam propagation method. The mode profiles were determined and the waveguides were fabricated by standard micro-fabrication techniques. Finally, the waveguides were tested. The single-mode chalcogenide strip-loaded shallow rib waveguides exhibited a low loss of ~ 1 dB/cm at wavelength of 980 nm.

Key words: chalcogenide glass, strip-loaded shallow rib waveguide, effective index method, finite difference method, beam propagation method

Simpler is Better

Acknowledgments

I would like to take this opportunity to express my deep gratitude to my supervisor **Dr. J. N. McMullin** and **Dr. Chris Haugen**, for giving me a chance to work in the wonderful optical world and for their guidance throughout this project. I really benefited from their advice and suggestions.

I would also like to thank **Professor Ray Decorby** for much help during this project.

I also owe a great deal of thanks to the following people for the help they have extended:

Hue Nguyen, TRILabs, for her hand-on training on micro-fabrication equipment and processes throughout this project;

Dr. Prabhat Dwivedi, TRILabs, for his assistant in making films;

Prof. Steve Dew, University of Alberta, for his advice on the fabrication process;

TRILabs Graduate Students - **Robert Bryce**, **Harini Gopaluni**, **Travis Robinson**, **Ponnampalam Nakeeran**, and **Valerie Hughes**, for their help and suggestions.

Finally, I thank my family and friends for their support and encouragement throughout this work.

Table of Contents

1. INTRODUCTION	1
1.1 THE DEMAND FOR INTEGRATED OPTICS	1
1.2 THE CHALLENGE OF INTEGRATED OPTICS	3
1.3 CHALCOGENIDE GLASSES – A GOOD CANDIDATE FOR INTEGRATED OPTICS	3
1.4 CHALCOGENIDE WAVEGUIDES - THE BASIC ELEMENT	4
1.5 THESIS OUTLINE	5
2. REVIEW OF OPTICAL WAVEGUIDE TECHNOLOGY	6
2.1 INTRODUCTION	6
2.2 WAVEGUIDE STRUCTURE AND CLASSIFICATION	6
2.3 WAVEGUIDE CONFIGURATIONS	8
2.4 OPTICAL WAVEGUIDE LOSSES	10
2.5 WAVEGUIDE MODELING TECHNIQUES	12
2.6 OPTICAL WAVEGUIDE FABRICATION TECHNIQUES	14
2.7 OPTICAL WAVEGUIDE CHARACTERIZATION TECHNIQUES	20
3. WAVEGUIDE DESIGN AND SIMULATION	24
3.1 INVERTED RIB CHALCOGENIDE WAVEGUIDES	24
3.1.1 DESIGN OF SINGLE-MODE RIB WAVEGUIDES	24
3.1.2 SIMULATION OF SINGLE-MODE RIB WAVEGUIDES	27
3.2 STRIP-LOADED SHALLOW RIB WAVEGUIDES	30
3.2.1 DESIGN OF STRIP-LOADED SHALLOW RIB WAVEGUIDES	31
3.2.2 SIMULATION OF STRIP-LOADED SHALLOW RIB WAVEGUIDES	36
3.3 BENDS AND SPLITTER	40
3.3.1 DESIGN OF SINE-BENDS AND Y-SPLITTERS	40

3.3.2	SIMULATION OF SINE-BENDS AND Y-SPLITTERS	42
3.4	MASK DESIGN	43
4.	WAVEGUIDE FABRICATION	44
4.1	INVERTED RIB WAVEGUIDE FABRICATION	44
4.1.1	FABRICATION PROCESSES	44
4.1.2	OBSTACLES IN FABRICATION	48
4.2	STRIP-LOADED SHALLOW RIB WAVEGUIDE FABRICATION.....	52
4.2.1	FABRICATION PROCESSES	53
4.2.2	DISCUSSION	57
5.	WAVEGUIDE TESTING	60
5.1	MODE PROFILE CHARACTERIZATION	61
5.1.1	MODE PROFILES	61
5.1.2	ANALYSIS	63
5.2	EVALUATION OF WAVEGUIDE LOSSES	63
5.2.1	LIGHT PROPAGATION (TOP IMAGES).....	63
5.2.2	LOSS MEASUREMENT	65
5.2.3	ANALYSIS	66
6.	OTHER EXPLORED CHG WAVEGUIDE STRUCTURES	68
7.	CONCLUSIONS	70
7.1	SUMMARY OF WORK	70
7.2	SUGGESTIONS FOR FUTURE WORK.....	70
	BIBLIOGRAPHY.....	72
	APPENDIX I.....	76
	APPENDIX II.....	78
	APPENDIX III.....	80

APPENDIX IV	82
APPENDIX V	85
APPENDIX VI	89
APPENDIX VII	90

List of Tables

Table 2.1: Comparison of wet etching and dry etching.....	18
Table 3.1: Proposed inverted rib waveguide dimensions.....	27
Table 3.2: Fabricated strip-loaded shallow rib waveguide dimensions.....	35
Table 3.3: Effective indexes of the proposed strip-loaded shallow rib waveguides.....	36
Table 3.4: Fabricated sine-bend dimensions.....	40
Table 3.5: Fabricated Y-splitter dimensions.....	41

List of Figures

Figure 1.1: GDP diagram showing the growth of ICT sector.....	2
Figure 1.2: Growth in R&D expenditure for ICT sector.....	2
Figure 2.1: Waveguide confinements.....	7
Figure 2.2: Five possible waveguide cross-sections.....	8
Figure 2.3: Straight waveguide.....	9
Figure 2.4: Curved waveguide	9
Figure 2.5: Y-branch.....	10
Figure 2.6: Sine-wave S-bend approach.....	12
Figure 2.7: Evaporation system scheme.....	15
Figure 2.8: Contact exposure scheme for optical lithography.....	17
Figure 2.9: Typical parallel-plate reactive ion etching system.....	19
Figure 2.10: Scheme for scattered light measurement.....	21
Figure 2.11: Experimental setup for mode profile characterization.....	22
Figure 3.1: Structure of inverted rib waveguide.....	25
Figure 3.2: Single-mode condition curve for rib waveguide ($h=3\ \mu\text{m}$).....	26
Figure 3.3: Fundamental mode profile of a proposed rib waveguide ($w=4\ \mu\text{m}$).....	28
Figure 3.4: Transverse field profile of a rib waveguide ($W=4\ \mu\text{m}$) at $z=36000\ \mu\text{m}$	29
Figure 3.5: Scheme of strip-loaded shallow rib waveguide.....	31
Figure 3.6: Single-mode condition curve for strip-loaded shallow rib waveguide.....	34
Figure 3.7: Effective index vs. etching depth.....	37
Figure 3.8: Fundamental mode profiles.....	39

Figure 3.9: Beam propagating in a sine-bend.....	42
Figure 4.1: Inverted rib waveguide fabrication receipt.....	48
Figure 4.2: Stress cracks a sample which had been sitting for 12 days.....	49
Figure 4.3: Deep-etching problem of As_2Se_3 film.....	51
Figure 4.4: SEM picture of a fabricated inverted rib waveguide.....	52
Figure 4.5: Clean-up can reduce pinhole and defect.....	54
Figure 4.6: Strip-loaded shallow rib waveguide fabrication receipt.....	56
Figure 4.7: SEM pictures of a fabricated strip-loaded shallow rib waveguide.....	57
Figure 4.8: Sample structure after TORLON etching.....	58
Figure 4.9: Horns and faceting in RIE.....	59
Figure 5.1: End coupling scheme.....	60
Figure 5.2: Intensity distribution of a waveguide output (horizontal direction).....	61
Figure 5.3: Intensity distribution of a waveguide output (vertical direction).....	62
Figure 5.4: Waveguide output images.....	62
Figure 5.5: Light propagating in a straight waveguide.....	63
Figure 5.6: Light propagating in a Y-splitter.....	64
Figure 5.7: Scattering loss vs. propagation distance.....	65
Figure 5.8: Field profiles of a fabricated waveguide and a single-mode fiber.....	66
Figure 5.9: Edge roughness of the fabricated waveguides.....	67
Figure 6.1: Laser-writing setup.....	69
Figure 6.2: Microscope picture showing a laser-writing waveguide.....	69

List of Acronyms and Abbreviations

MEMS	Micro-Electro-Mechanical Systems
TRLabs	Telecommunication Research Laboratories
GDP	Gross domestic product
WDM	Wavelength division multiplexing
CHG	Chalcogenide glass
UV	Ultra-violet
SEM	Scanning electron microscope
RIE	Reactive ion etching
IC	Integrated circuit
DC	Directional current
FD	Finite difference
BPM	Beam propagation method
EI	Effective index
MEA	Monoethanolamine
EDA	Ethylenediamine
PR	Photo-resist
dB	decibel
IR	Infrared

1. Introduction

1.1 The demand for integrated optics

Integrated optics generally means to guide and manipulate light in micron-scale dielectric waveguides. The reason to miniaturize optics is the same as in integrated electronics: to achieve lower cost, higher efficiency and higher performance.

Integrated optics is a concept that was brought to us 30 years ago. Early in 1969, Miller [1] pointed out it is inconvenient to place and align all optical components on light benches and suggested the idea of integrated optics. After that, great effort was made to compress different functions into one single chip.

At the beginning, the field of integrated optics grew very slowly. However as more and more governments, universities and research labs have become involved, this field has increased at a rapid rate due to the booming of the information and communication industries, which are the main application areas of integrated optics. As seen in Industry Canada's statistical data [Figure 1.1], the GDP of the Information and Communication industries increased 180% between 1997 and 2000, which is much faster than the growth of Canadian economy during the same period.

Obviously, the basic reason for the development of integrated optics is profit. Optical fibers are well developed and widely used, and nowadays most of the investment for wavelength division multiplexing system (WDM) goes into optical devices, such as filters, switches etc. No doubt there is a high demand for integrated optics, and as a result, companies have increased their research and development expenditures [Figure 1.2] rapidly in recent years.

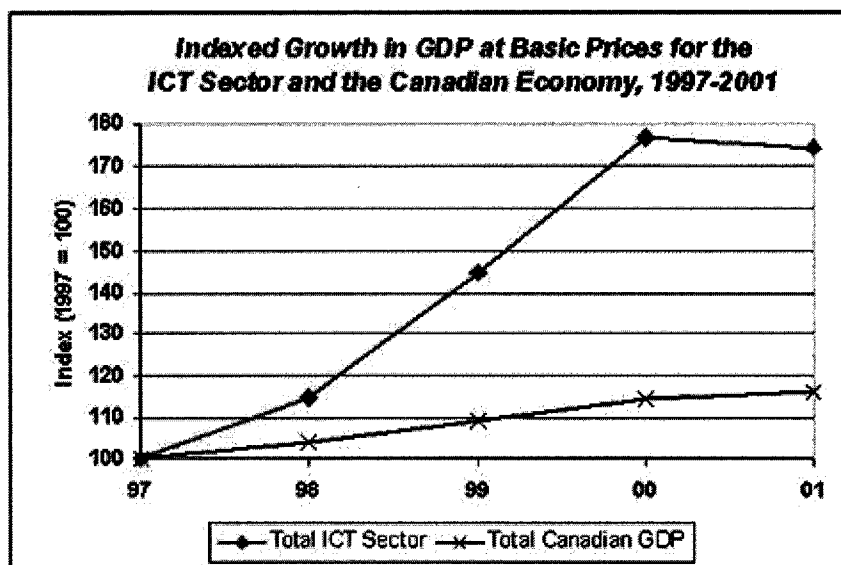


Figure 1.1: GDP diagram showing the growth of ICT sector

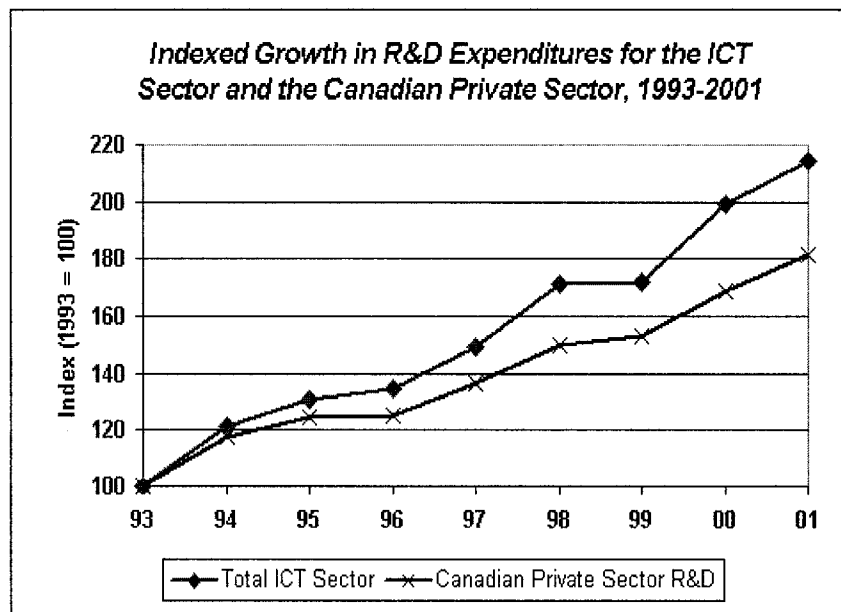


Figure 1.2: Growth in R&D expenditure for ICT sector

* ICT: Information and Communication Technologies

1.2 The challenge of integrated optics

For the information and communication industries, the most important functions that are required for high-speed, mass-producible photonic and optoelectronic circuits are:

- Waveguides, including straight waveguides, curved waveguides and Y-branches
- Couplers, optical filters and switches
- Multiplexers and Demultiplexers
- Optical sources and sensors
- Optical modulators and amplifiers

Ideally, all of these functions would be integrated into a single chip. However, since each of these functions tends to have its own ‘optimal’ material system [2], this goal still has a long way to go. With current technology, III-V semiconductors are favored as light sources, modulators work best in lithium niobate and passive devices (waveguides, mux etc.) are fabricated in SiO₂. Thus, integrating many functions into one single chip is still a challenge. To achieve such monolithic integration, scientists are trying to modify the properties of a single material system or develop ways to integrated diverse materials on a single platform (i.e. a single chip).

1.3 Chalcogenide glasses – a good candidate for integrated optics

Glasses, which lack the long-range periodicity characteristic of crystals, have long been manipulated to achieve multi-functions. For example, glass fibers can be doped with erbium to make an amplifier (erbium-doped fiber amplifier).

Chalcogenide glasses (CHGs), glasses that contain one or more of the elements from Group VI of the periodic table, namely S, Se or Te, have attracted great interest in recent years. In 1954, Kolomiets [3] discovered that chalcogenide glasses can act as semiconductors. Since then, these glasses have been used in several commercial applications, e.g. X-ray detection, photocopier.

Chalcogenide glasses are excellent candidates for integrated optics because they have the following properties [3]:

- Wide optical transmission band with potentially low loss for both 1.3 and 1.55 micron telecommunication windows [4];
- Photoluminescence and photoconductivity;
- Photo-darkening effect;
- Reversible structural changes;
- Large non-linear optical effects.

Thus it may be possible to integrate many functions into a single chip using chalcogenide glasses to make efficient and reliable devices. And the fabrication processes are compatible with the existing semiconductor industry.

1.4 Chalcogenide waveguides - the basic element

Current research on chalcogenide glasses is mainly in optical sources, micro-lenses, photo detectors and optical memories [5]. Few experiments have been performed on chalcogenide waveguides. Since the basic element of all passive and active optical devices is the waveguide, further research on chalcogenide waveguides should be done. Also, the availability of high quality chalcogenide glasses as well as the capability of fabricating optical devices using

thin film technology will facilitate the realization of relatively low cost waveguides.

1.5 Thesis outline

The goal of this thesis is to investigate the feasibility of making waveguides in Chalcogenide glass. Waveguide technology, including the state-of-the-art fabrication techniques and waveguide characterization techniques, is reviewed in Chapter 2. Chapter 3 is dedicated to the design and simulation of As_2Se_3 strip-loaded shallow rib waveguides. Fabrication and testing of these waveguides are described in Chapter 4 and 5 respectively. Chapter 6 briefly reviews my other research on As_2Se_3 laser-writing channel waveguides. Finally, a summary is presented in Chapter 7.

2. Integrated optical waveguide technology

2.1 Introduction

Light is important for the field of communications. In communications, bandwidth is generally proportional to the carrier frequency. Light has frequencies in the range $2 - 4 \times 10^{14}$ Hz. Therefore, compared to lower frequency radio waves, microwaves and millimeter waves, which also carry information in a way similar to light, light has the advantage of a potentially huge information carrying capacity.

However, free space optics is not suitable for communication for distances more than a few kilometers [6] because it suffers from scattering by rain, snow, dust and clouds, and as a result, has large attenuation. In addition to attenuation, the turbulence of air introduces large amounts of noise as well. Also, light propagating through the atmosphere diverges because of diffraction, which will lead to intensity loss in the central part of the beam. Thus, it is necessary to guide the light so that the power of the beam is confined in the transverse direction with minimized attenuation and noise. Devices which achieve this are normally called optical waveguides.

2.2 Waveguide structure and classification

In general, the most common form of optical waveguide consists of two regions: a region called the core, which has a higher refractive index, and the surrounding area called the cladding, which has a lower refractive index.

Optical waveguide structures can be categorized as step-index or graded-index. For step-index waveguides, the refractive index is constant within the confinement region, while for the graded-index waveguide, the refractive index is a function of the coordinates and thus varies both inside and possibly outside of the confinement region [7].

According to the number of spatial dimensions that provide confinement, waveguides can also be classified into one-dimensional (1D) waveguides and two-dimensional (2D) waveguides as shown in Figure 2.1. One-dimensional waveguides, called slab waveguides, have few practical applications. Currently, 2D waveguides formed on a substrate are of great interest in integrated optics because light can be guided between specific points on a substrate.

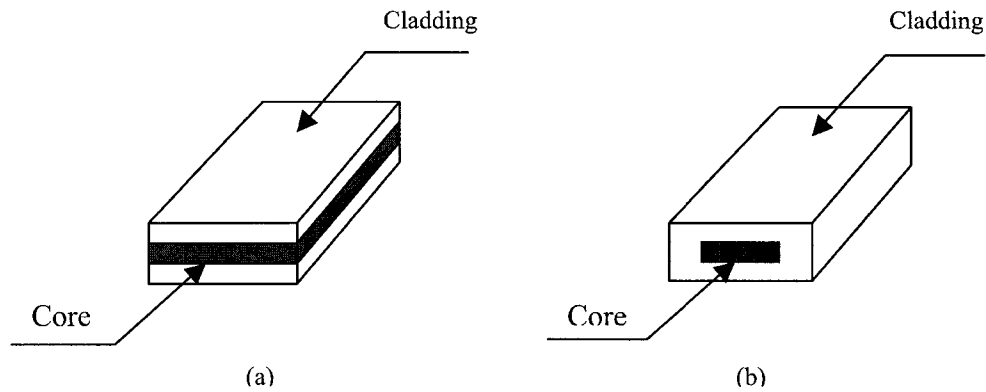
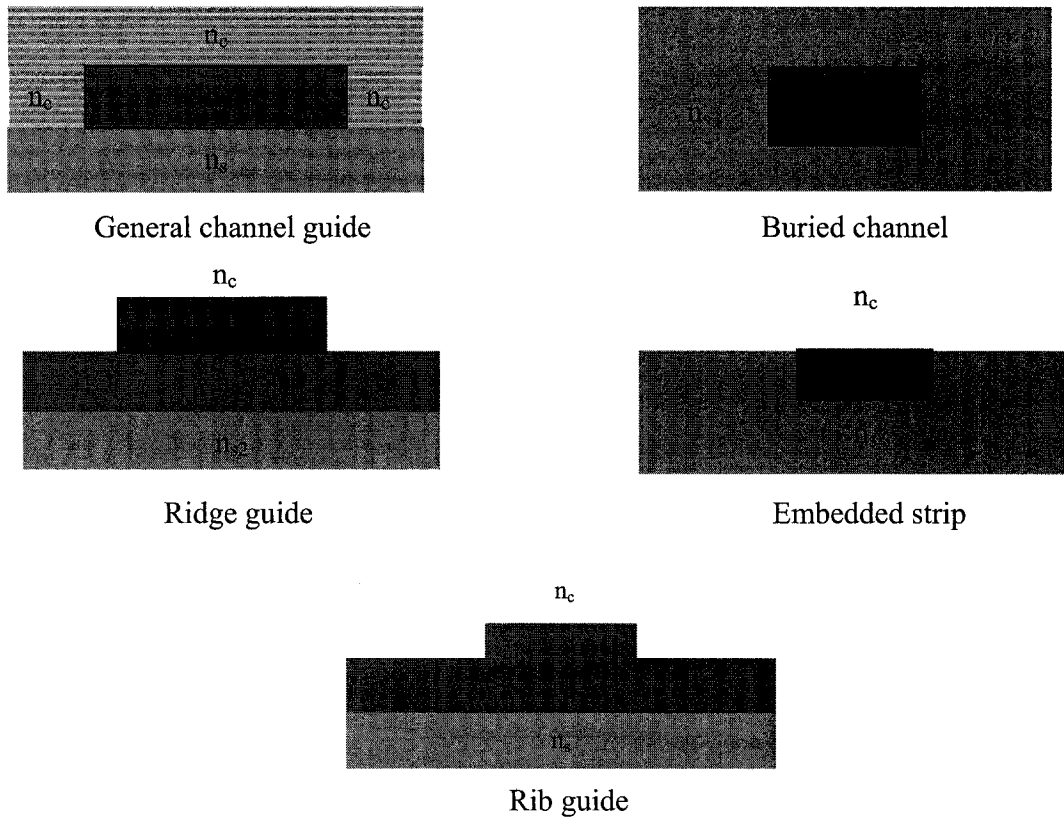


Figure 2.1: Waveguide confinements: (a) 1D confinement; (b) 2D confinement

For design and simulation purposes, 2D waveguides using standard thin film techniques can be treated as rectangular waveguides. There are many configurations as seen in Figure 2.2.



* $n_f > n_c, n_s$ (n_c : cladding index; n_f : core index; n_s : substrate index)

Figure 2.2: Five possible waveguide cross-sections

2.3 Waveguide configurations

In integrated optical circuits, light is manipulated in different ways to achieve different functions. The basic function of waveguides is guiding light between locations in a micro-system. Thus, the main passive waveguide configurations include:

- Straight section: To guide the light in a direct route [Figure 2.3].

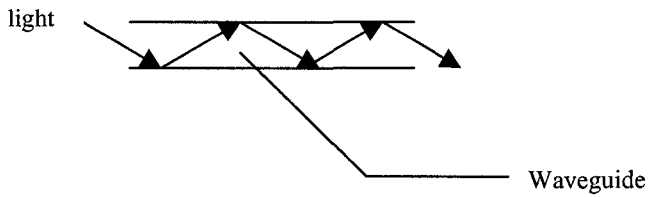


Figure 2.3: Straight waveguide

- Curved section: To change the propagation direction of light in order to guide light between any points in an integrated circuit [Figure 2.4].

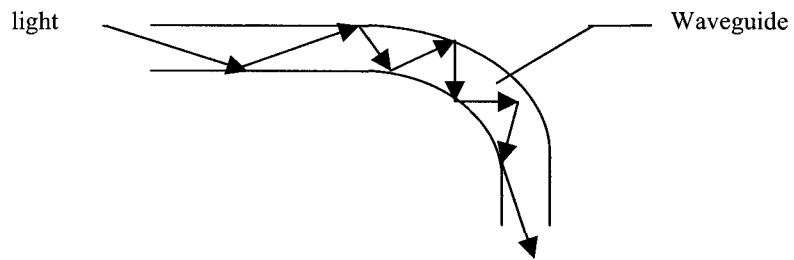


Figure 2.4: Curved waveguide

Curved waveguides are necessary to reduce the length of integrated optical components and circuits. As discussed later in this chapter, if the curve radius is too small, the light will radiate out. Many different shapes have been tried in order to minimize the bend losses.

- Splitter: To divide light in order to direct a signal to two or more parts in an integrated optical circuit.

Splitters tend to be very long with a very small separation angle. This is to avoid high losses, just as in the curved section. Compared to other types of splitters, Y-branches [Figure 2.5] are simpler, thus more practical.

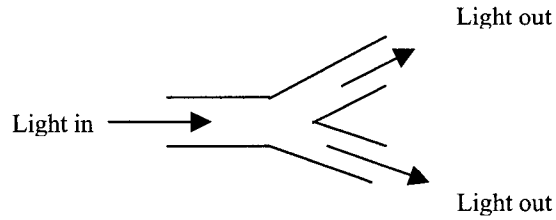


Figure 2.5: Y-branch

2.4 Optical waveguide losses

The fabrication of low loss optical circuits is necessary because the usefulness of optical devices is determined largely by their losses. High loss waveguides often limit the device performance. In most practical applications, the waveguide propagation losses should be less than 1 dB/cm [7].

The losses of integrated optical waveguides can be classified into two major categories according to their mechanism [7]:

1. Absorption

The absorption loss is due to the optical energy being dissipated or converted into other form of energy as a result of its interaction with waveguide material. There are three kinds of absorption loss: intrinsic, impurity and atomic defects.

For current optical materials, absorption loss can be minimized in the waveguide range of interest, namely 800 to 1600 nm, the “IR window”. Chalcogenide glasses in the IR window have very low absorption losses.

2. Scattering loss

The scattering loss is due to the conversion of guided optical light into radiation modes or other guided modes. Scattering loss [7] can be caused by

imperfections (the compositional variations within the volume of the waveguide or dimensional fluctuations associated with variations in the height and/or width of the waveguide), which result in density and refractive index fluctuations. Even though the scattering loss has been substantially reduced to the fundamental limit in fibers, it is still important in integrated optics. Specifically, scattering loss in chalcogenide glass waveguides could be due to the growth of microscopic crystals that have higher density at the glass/air interface during the evaporation step [5]. Thus, special treatment for example, annealing, of the sample is necessary.

Radiation loss caused by directional changes is another issue that should be considered in integrated optical circuit design. This plays an extremely important role in determining the density of components on a single integrated optic substrate, and is the reason why optical devices tend to be very long and narrow currently.

The loss in the bend or splitter section is due to the mode mismatch [8]. To predict bending loss accurately, an accurate description of the fundamental mode field of the waveguide and the waveguide parameter is required. For the curved regions connecting two parallel waveguides (directional coupler and Mach-Zehnder interferometer for example), the result of Minford et al. [9] can be used in practice, so that extensive theoretical discussion can be avoided.

What Minford derived is as follows: for the connection of two parallel waveguides, if the length of the curved section is l_x and the offset of the two parallel waveguides is l_y , sine-wave S-bend [Figure 2.6] is generally the optimal solution, as specified by the following piece-wise continuous equation:

$$y = \left(\frac{l_y}{l_x}\right)x + \frac{l_y}{2\pi} \sin 2\pi\left(\frac{x}{l_x}\right) \quad (2.1)$$

If the radius of curvature varies gradually in the sine-bend (continuous second order derivative), mode mismatch is minimized at each point. The typical loss of sine-wave s-bend is less than 0.2 dB for $l_x/l_y > 100$ [10].

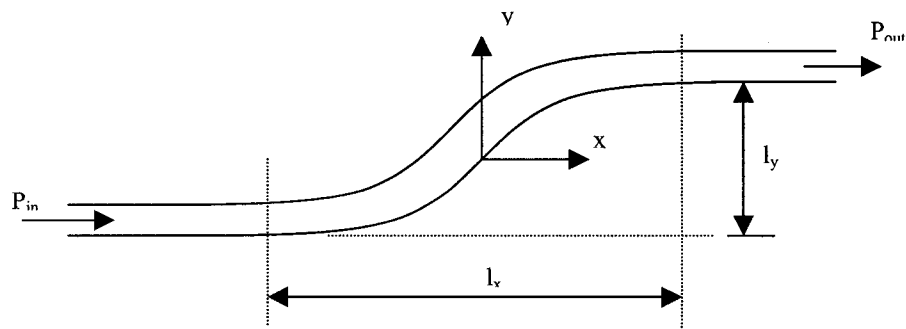


Figure 2.6: Sine-wave S-bend approach

There is always a tradeoff in the design of a sine bend. The more tightly confined a mode is, the smaller bend radius can be accepted. In the case of a rib waveguide, this means a large index offset between center region and the outside regions is required. The larger the index offset is, the smaller the guide should be to maintain single mode condition, thus the more difficult to launch light from a fiber to the waveguide.

2.5 Waveguide modeling techniques

Simply speaking, light in a waveguide can be viewed as being confined in one or more dimensions along the propagation direction by total internal reflection [11]. Total internal reflection, or TIR, is the reflection of the total amount of incident light at the boundary between two mediums.

Historically, geometrical optics analysis has been applied for waveguides with dimensions greater than the wavelength of light [6] in order to describe the phenomenon of guidance by total internal reflection. However, when the dimension of the waveguide approaches the wavelength of light, the solution of Maxwell's equations is necessary to analyze waveguides. Thus, waveguide modeling generally means to figure out the solution of the following Helmholtz equation that is derived from Maxwell's equations for each isotropic, lossless dielectric medium, and then use the boundary conditions to match the solutions at the boundaries between these media [2, 12].

$$\nabla^2 \vec{e} = -\omega^2 \mu \epsilon \vec{e} = -k^2 \vec{e} \quad (2.2)$$

$$\nabla^2 \vec{h} = -\omega^2 \mu \epsilon \vec{h} = -k^2 \vec{h} \quad (2.3)$$

Here: $e = E_0 e^{i(\omega t - k_x x - k_y y - k_z z)}$ is the electric field, $h = H_0 e^{i(\omega t - k_x x - k_y y - k_z z)}$ is the magnetic field (E_0 and H_0 represent the amplitude of the field); $k^2 = k_x^2 + k_y^2 + k_z^2 = \omega^2 \mu \epsilon$ (k_x, k_y, k_z are the propagation constants along the x, y and z directions respectively); and $\omega = 2\pi c / \lambda$ (c is the light velocity in free space), $\epsilon = \epsilon_r \epsilon_0$ is the permittivity of the dielectric (ϵ_r is the relative permittivity of the dielectric, ϵ_0 is the permittivity of vacuum), $\mu = \mu_r \mu_0$ (μ_r is the relative permeability of the dielectric, μ_0 is the permeability of vacuum).

Unfortunately, except the slab waveguide, which has a simple structure for which exact closed form solutions exist, directly solving Maxwell's equation to get the mode profiles is generally impossible. Solutions are then sought by solving Maxwell's equations using either numerical or semi-analytical methods.

Several numerical and semi-analytical methods have been developed so far. Among them, finite difference, beam propagation and effective index methods have proven to be accurate, efficient and stable.

While a finite difference method (FD) is typically used to figure out the lateral mode profiles (the X-Y shapes of the field), the beam propagation method (BPM) describes the evolution of the total field along the direction of propagation, Z, in a waveguide [13]. This can be simply stated as: Given the optical field at the input plane $Z=0$ (for example, the field coupled into the integrated optical circuit from the input fiber), and the known refractive index distribution of the waveguide circuit, what is the optical field through the optical circuit. Combining FD with BPM (FD-BPM) can give a detailed picture of the light in a waveguide.

There are several reasons for the popularity of FD-BPM in modeling optical guides like tapers, bends, splitters and gratings. Perhaps the most significant one is that it is easy to use and can be applied to complex geometries without having to develop specialized versions of the method [14] while maintaining high efficiency. Thus an understanding of the proper usage and results of the tool can be readily grasped by a non-expert in numerical methods [15].

On the other hand, the effective index (EI) method [14], which calculate the approximate propagation constants in a waveguide by decomposing the two-dimensional waveguide problem into two separated one-dimensional waveguide problems (See Appendix I for a summary of EI method), is widely used for deriving the mode profiles, because it has advantages in simplicity, accuracy and speed.

With the improvement in computer technology, commercial CAD packages using the FD, BPM and EI methods are available nowadays to provide accurate, fast and efficient analyses of micron-size waveguides with different structure and configuration.

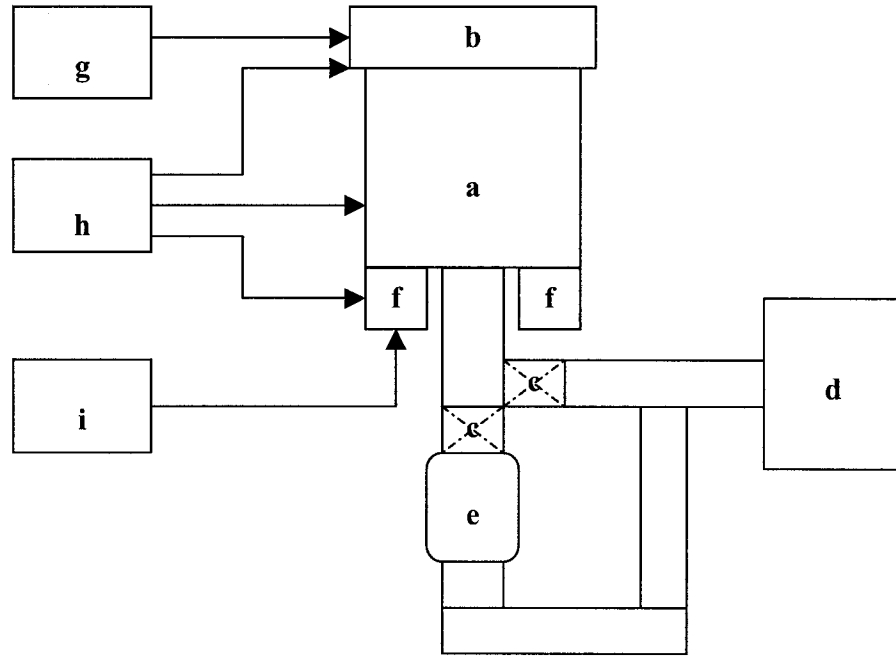
2.6 Optical waveguide fabrication techniques

Since the term “integrated optics” originated in 1969 [1], many waveguide fabrication techniques have been proposed and used to form various optical

waveguides on different substrate materials. The usefulness of these waveguides is determined largely by their mechanical and optical properties.

Some of the latest fabrication processes that are related to this project are summarized as followed:

➤ Evaporation



a: vacuum chamber
d: mechanical pump
g: thickness monitor

b: chamber cover and substrate holder
e: diffusion pump
h: cooling system

c: valve
f: electrode
i: power supply

Figure 2.7: Evaporation system scheme

The basic idea for evaporation is to heat the material to be deposited in a vacuum chamber until it evaporates. The vapor then condenses on the cooler substrate to form the film.

Evaporation techniques have been employed in the optical field for a long time and are still used today because of their simplicity. However, evaporation has its shortcomings. The films made by evaporation have poor sidewall coverage and relatively low density and small grains. Moreover, compared to sputtering, evaporation films in which atoms arrive with a lower energy have worse adhesion [16], thus careful annealing is necessary. Annealing can also get rid of the intrinsic stress inherent in evaporated films.

A typical evaporation system is composed of three main parts as shown in Figure 2.7. First is the pumping system, which consists of a diffusion pump and a mechanical pump. The pressure is maintained at around 10^{-6} Torr. Low pressure is required so that the vapor travels from source to substrate with minimal collisions with gas molecules. Otherwise, the film quality is poor, the deposition rate is low and source utilization is low. Moreover, the vacuum system protects the contamination of the surface from the ambient surroundings.

The second is the vacuum chamber which consists of a refractory “boat”, electrical heating system and cooling system. The heating system is composed of two pairs of electrodes, and the evaporating speed is controlled by manipulating the voltage between the electrodes. The microscopic roughness of the surface depends on by evaporating speed and system temperature.

The third part of the system is the substrate holder and a cover for the vacuum chamber which include a crystal thickness monitor to measure the thickness of the film. The deposition rate is determined by the emitting flux and by the geometry of the target and the substrate holder [17].

➤ Optical lithography

The performance and size of the optical chips are partly dictated by the lithographic minimum printable size. Lithography, which replicates a pattern

rapidly from wafer to wafer, or substrate to substrate, also determines the throughput and the cost of optical systems. A lithographic system includes exposure tool, mask, resist, and all of the processing steps to accomplish pattern transfer from a mask to a resist and then to devices.

Although e-beam and x-ray systems are at present the primary lithographic technique used in sub-quarter-micron device research due to their intrinsic high resolution, optical sources remain attractive because of their high wafer throughput, and they are the only ones used commercially. The dominance of optical lithography is the result of a worldwide effort to improve optical exposure tools and resists. For features over 1 μm , optical lithography is adequate [16].

A typical optical lithography system using the contact method, in which mask and wafer are held in intimate contact by a vacuum after careful alignment with existing features, is illustrated in Figure 2.8.

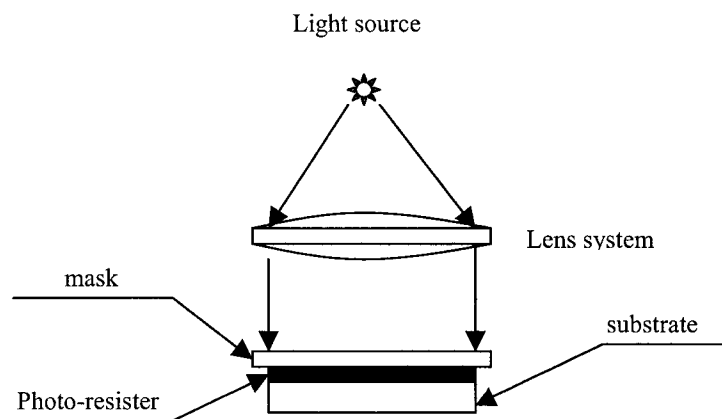


Figure 2.8: Contact exposure scheme for optical lithography

- Reactive ion etching

It is necessary to etch the thin film previously deposited and/or the substrate itself in order to form a functional structure on a substrate. Etching is a micro-fabrication process for transferring the pattern that is defined by a mask prepared by lithographic techniques on layers of photo-resist. In general, there are two classes of etching processes:

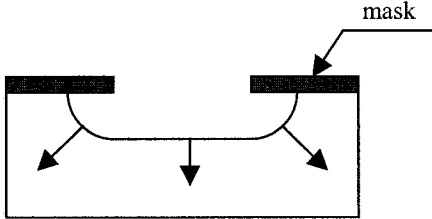
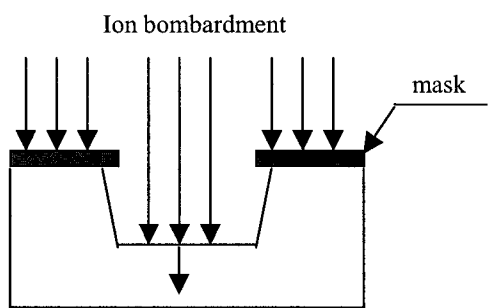
<i>Wet Etching</i>	<i>Dry Etching</i>
<p>Disadvantage:</p> <ol style="list-style-type: none"> 1. Isotropy  <p>Advantage:</p> <ol style="list-style-type: none"> 1. Simple 2. High etching rate 3. Low cost 	<p>Advantage:</p> <ol style="list-style-type: none"> 1. Large anisotropy  <p>Disadvantage:</p> <ol style="list-style-type: none"> 1. Low selectivity 2. Low etching rate 3. Increased cost and complexity

Table 2.1: Comparison of wet etching and dry etching

1. Wet etching, which is the simplest approach by immersing the wafer into a chemical solution that preferentially removes the underlayer without substantially degrading the PR pattern [18].

2. Dry etching, where the underlayer is dissolved by reactive ions or a vapor phase etchant.

As seen from Table 3.1, the main advantage of dry etching is the possibility of anisotropic etching due to ion bombardment [16]. This process is optimized in a variant of plasma etching called reactive ion etching (RIE).

In RIE, the substrate is placed inside a reactor in which several gases are introduced. An RF power source generates a plasma in which the gas molecules dissociate into ions. The ions are strongly accelerated and impinge vertically on the substrate. If the ions have enough energy, they can knock atoms out of the material to be etched. This is the physical part of RIE. There is also a chemical part, in which the ions also react at the surface of the material being etched and form another gaseous material that can be pumped away. A schematic of a typical RIE system is shown in Figure 2.9 below.

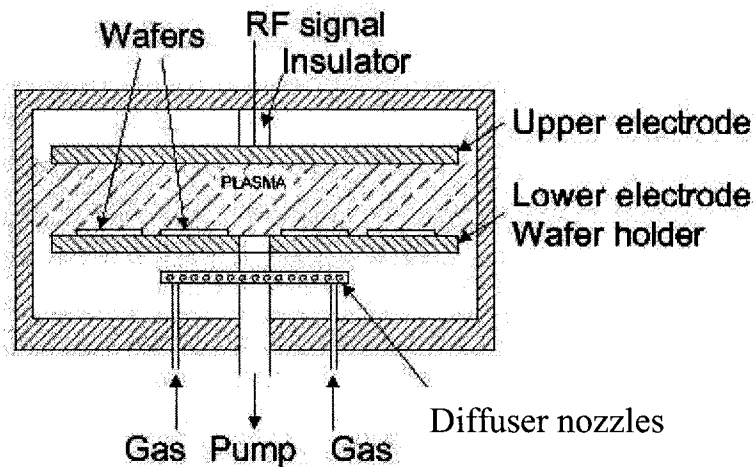


Figure 2.9: Typical parallel-plate reactive ion etching system

There is a trade-off between the chemical and physical etching, and the RF voltage and gas content needed to be adjusted, since the chemical part

creates a smooth surface, but is isotropic and tends to cause undercutting, while the physical part is anisotropic, creates vertical sidewalls, but tends to create a rough surface.

2.7 Optical waveguide characterization techniques

Waveguides are the basic element in an integrated optical circuit. An accurate knowledge of the optical characteristics, especially the propagation losses and mode profiles of these waveguides is necessary for device design and specification, as they characterize the quality of a waveguide.

1. Loss measurement

The losses in a waveguide can be caused by absorption, scattering and bend, as discussed in Section 2.4. The attenuation coefficient, α , which describes the losses in a waveguide, is given by

$$\alpha = \frac{10 \log(P_0 / P_1)}{z_1 - z_0} (dB / cm), \quad (2.3)$$

where P_0 and P_1 are the optical power at the positions z_0 (cm) and z_1 (cm) in the waveguide respectively. Therefore, to measure the attenuation involves measuring the transmitted light as a function of propagation distance. Prism coupling and cutback are two commonly used methods.

Instead of measuring the transmitted light, one can measure the scattered light. In an optical waveguide, a guided mode continuously loses a small part of its power by Rayleigh scattering. This scattered power is assumed to be proportional to the total guided power, thus

$$\alpha = \frac{10 \log(P_{scatt0} / P_{scatt1})}{z_1 - z_0} (dB / cm), \quad (2.4)$$

where $P_{\text{scatt}0}$ and $P_{\text{scatt}1}$ represent the measured scattered light at z_0 and z_1 . The decrease in scattered light shows the propagation losses of the guided mode.

The experimental setup to detect the scattered light is shown in Figure 2.10. It includes a video camera, a video monitor, a video camera controller with an A/D converter and a computer. When the light scattered from the waveguide is detected by the video camera, the light intensity profile can be measured and the scattered light power can be found in terms of the propagation distance. Typically, the scattered light decreases exponentially along the waveguides (constant α), and the attenuation coefficient is obtained by fitting the measured scattered power to a decreasing exponential function. The computer can help to do this, as well as control the camera. The accuracy depends on the sensitivity of the detection system.

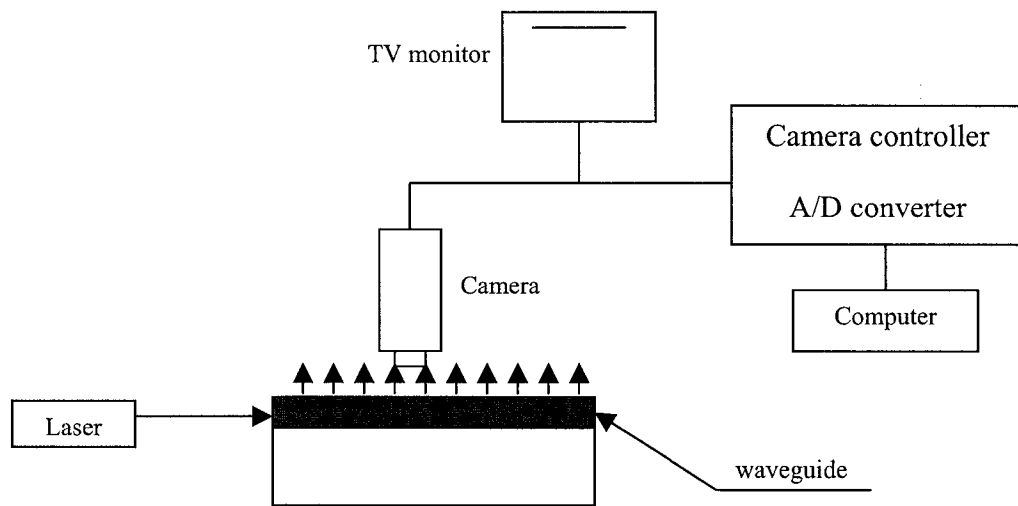


Figure 2.10: Scheme for scattered light measurement

Compared to other loss measurement methods, the scattered light measurement is a more useful technique, as it determines the propagation losses of

a waveguide without destroying it, and can be used for channel waveguides. Light propagation in devices such as bends, Y-branches can also be observed using this scattered light measurement method.

2. Mode profile characterization

The mode profile, or more specifically the intensity distribution of a mode, is related to many properties of the waveguide such as its coupling coefficient to an optical fiber or another waveguide, and its interaction with a grating. Thus the mode profile is an important characteristic of a waveguide. Through mode profile characterization, the number of modes, as well as mode dimensions and the symmetry of the waveguide can be derived.

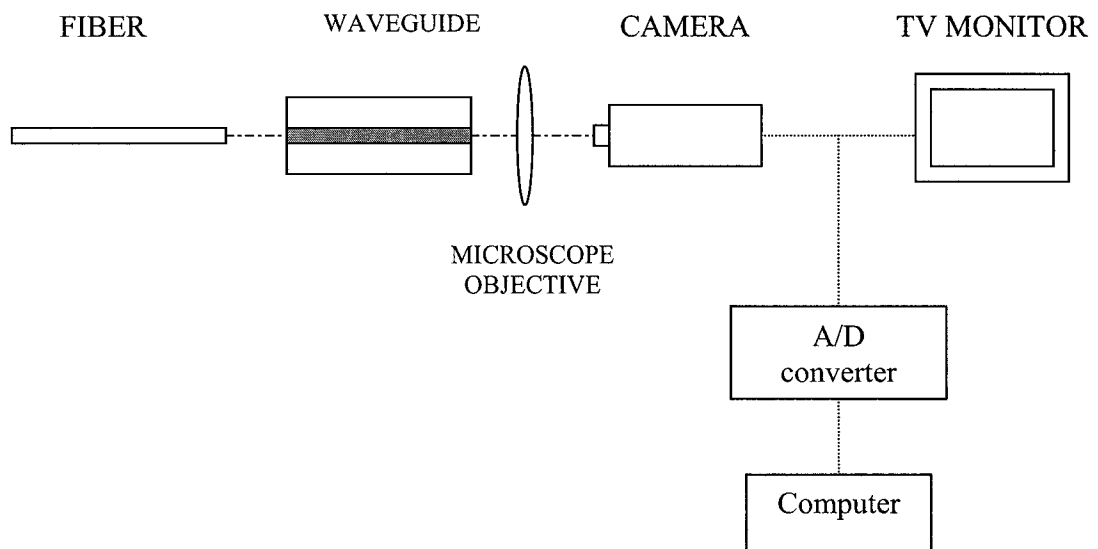


Figure 2.11: Experimental setup for mode profile characterization

A typical experimental setup for mode profile characterization is shown in Figure 2.11. Light from an optical fiber is end-coupled into a waveguide. Because

waveguide dimensions are in the micrometer range, light coming out of the waveguide is put through a microscope objective, and the near field pattern is magnified. The image is then focused onto a video camera and converted to digital data that can be processed by a computer.

One obstacle to get correct mode profiles with this setup might be the linearity of the camera. The camera should have a very good linear response to the optical power, or the mode profiles will be distorted.

3. Waveguide design and simulation

For our experiments, arsenic tri-selenide (As_2Se_3) was used. This chalcogenide material was selected because it has good transparency at 1550 [3]. Moreover, it is a readily available material.

In this chapter, the design of waveguides in As_2Se_3 is presented. Also, the simulation results of these waveguides are discussed in terms of confinement and mode shape.

3.1 Inverted rib chalcogenide waveguides

3.1.1 Design of single-mode rib waveguides

Considering the large index offset between As_2Se_3 and typical cladding materials (e.g. SiO_2), large cross-section rib waveguides, a novel waveguide concept proposed by Marcatili [19], were initially considered. This design allows for a large cross-section of single-mode waveguides despite the big difference in refractive index between core and cladding material. Thus, a lower coupling loss to fiber and a lower propagation loss can be obtained.

At first glance, the rib waveguide structure may be confusing since there are no physical core-cladding boundaries in the horizontal direction. However, rib waveguides do have transverse confinement due to the effective index offset between the center region and the side regions [20]. The effective index offset is relatively small. By properly defining the proportional size of transversal dimensions, mono-mode rib waveguides can be comparable to single-mode optical fiber. This consequently provides better coupling between waveguide and fiber.

Rib waveguides have been analyzed extensively in [20 – 29]. The result of Pogossian et al. [20] have a simple normalized form, and can be used for the analysis in this project.

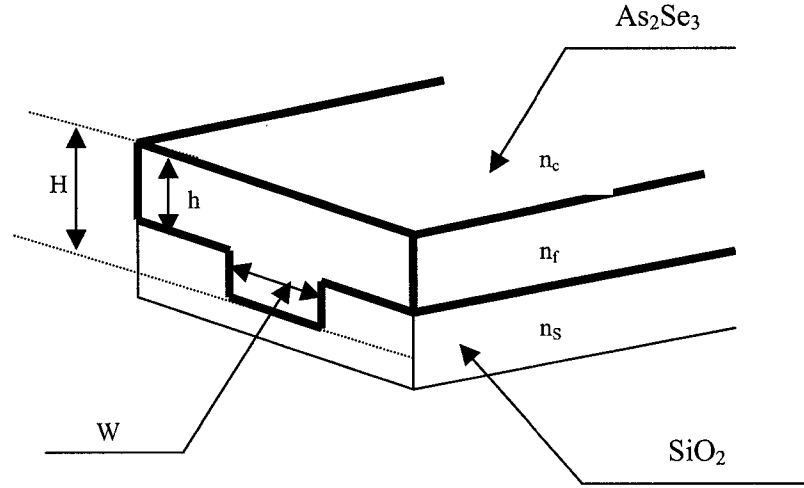


Figure 3.1: Structure of inverted rib waveguide

A schematic diagram of the proposed waveguide structure is shown in Figure 3.1. The inverted structure was used, thus both As_2Se_3 etching and additional effort can be avoided. Air was used as the upper cladding, and SiO_2 as the substrate. Therefore, total internal reflection can be maintained since both have an index of refraction lower than As_2Se_3 .

For the rib structure in Figure 3.1, the conditions that Pogossian et al [20]. derived for single-mode propagation can be formulated as follows:

$$t < \frac{r}{(1-r^2)^{1/2}}, \quad (3.1)$$

$$r(= h_{eff} / H_{eff}) > 0.5 \quad (3.2)$$

Defining $t = \frac{W_{eff}}{H_{eff}}$, and $r = \frac{h_{eff}}{H_{eff}}$,

Where: $h_{eff} = h + q$, $H_{eff} = H + q$,

$$W_{eff} = W + \frac{2\gamma_c}{k(n_f^2 - n_c^2)^{1/2}},$$

$$q = \frac{\gamma_c}{k(n_f^2 - n_c^2)^{1/2}} + \frac{\gamma_s}{k(n_f^2 - n_s^2)^{1/2}},$$

n_f, n_s, n_c are the refractive indices of the core, lower cladding and the upper cladding respectively (see Fig.2 for detail),

For TE modes, $\gamma_{c,s} = 1$; for TM modes, $\gamma_{c,s} = \left(\frac{n_{c,s}}{n_f}\right)^2$,

$k = \frac{2\pi}{\lambda}$, λ is the wavelength.

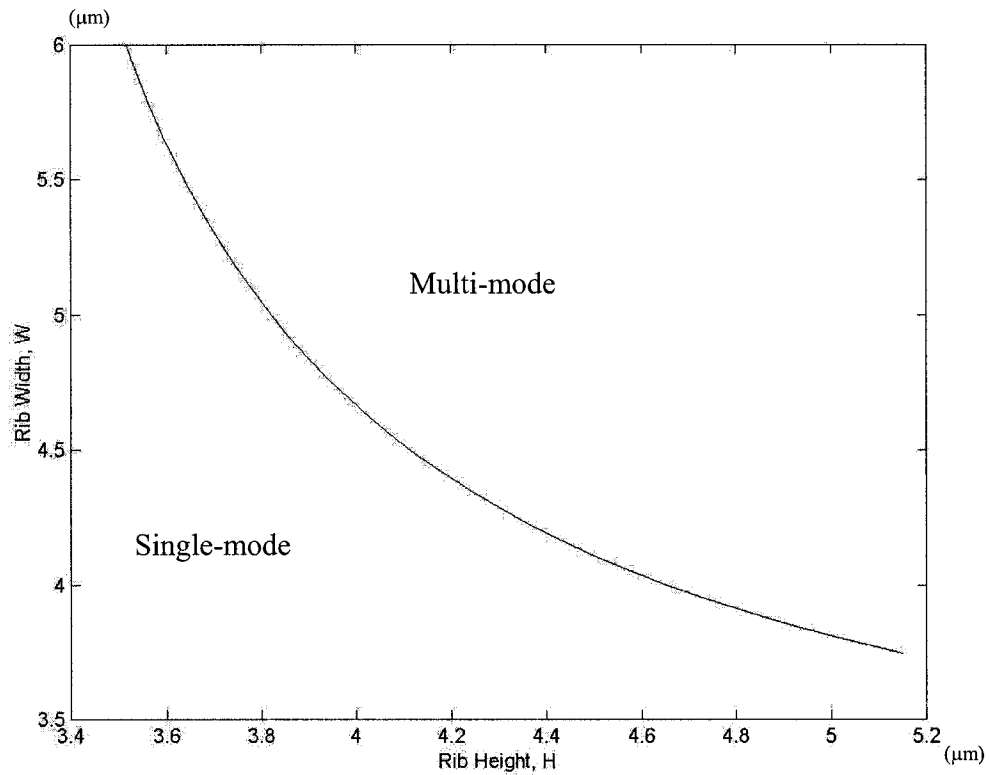


Figure 3.2: Single-mode condition curve for rib waveguide (h=3 μm)

Equation (3.1) and (3.2) tell us that whether the rib waveguide only supports fundamental mode depends largely on the ratio of the rib width to the rib height. A plot of H as a function of W for h=3 micron is shown in Figure 3.2. The region under the curve corresponds to mono-mode propagation, while the region above the curve is the multi-mode zone.

The following single-mode points which have maximum W/H for the given h were selected for fabrication.

	1	2	3	4	5	6	7	8
W (μm)	4.5	4.4	4.3	4.2	4.1	4.0	3.9	3.8
H (μm)	4	4.1	4.3	4.2	4.3	4.5	4.6	4.8
h (μm)	3	3	3	3	3	3	3	3

Table 3.1: Proposed inverted rib waveguide dimensions

3.1.2 Simulation of single-mode rib waveguides

It is necessary to verify the single-mode propagation of the designed waveguides and to evaluate the mode profiles and other theoretical parameters before fabrication. The commercial software packages tempSelene and BeamPROP [15] were used in this project to derive the fundamental mode profiles and to confirm the single-mode propagation.

a) Fundamental mode profiles

The fundamental mode shapes were derived by running the Mode Cal in tempSelene [finite difference method: ncore=2.72; nup=1; ndown=1.45; H, h and

W are as illustrated in Table 3.1; substrate thickness=10 μm ; calculation window: 50 μm X 50 μm]. The simulation result is shown in Figure 3.3.

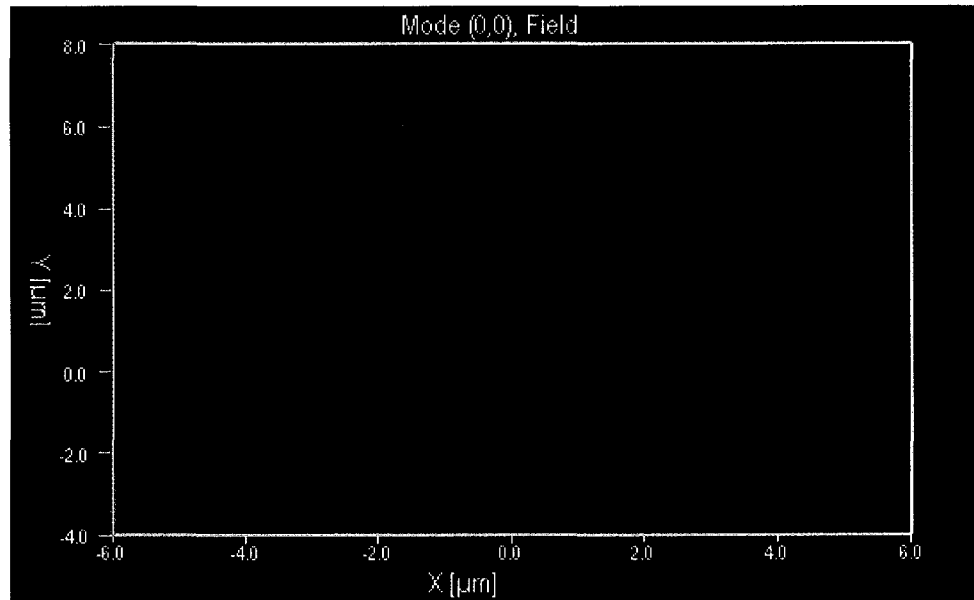


Figure 3.3: Fundamental mode profile of a proposed rib waveguide ($w=4 \mu\text{m}$)

Figure 3.3 tells us rib waveguides do have lateral confinement, as seen from the plot that large amount of power carried by the fundamental mode (illustrated by the red circle) is confined under the rib.

Figure 3.3 also tells us the proposed rib waveguides have good coupling efficiency to single-mode fibers, in view of the fact that the amount of power coupled to a waveguide is determined by how similar the input field distribution is to the transverse field profile of the fundamental mode of the waveguides [10]. As shown by the simulation software, the fundamental mode of the proposed rib waveguides has an approximate gaussian distribution both in lateral and vertical direction with full width half maximum (FWHM) around $3.26 \mu\text{m}$ and $2.30 \mu\text{m}$ respectively. Because the input field from a single-mode fiber to waveguides is

an approximate gaussian beam, the proposed rib waveguides are matched to single-mode fibers in terms of shape and mode field diameters.

TempSelene did find the designed rib waveguides support high order modes in the FD point of view. However, as stated by Pogossian et al. [20], since the single-mode conditions are met, the high order modes will radiate out when light propagates through the rib waveguides.

b) Verification of single-mode behavior

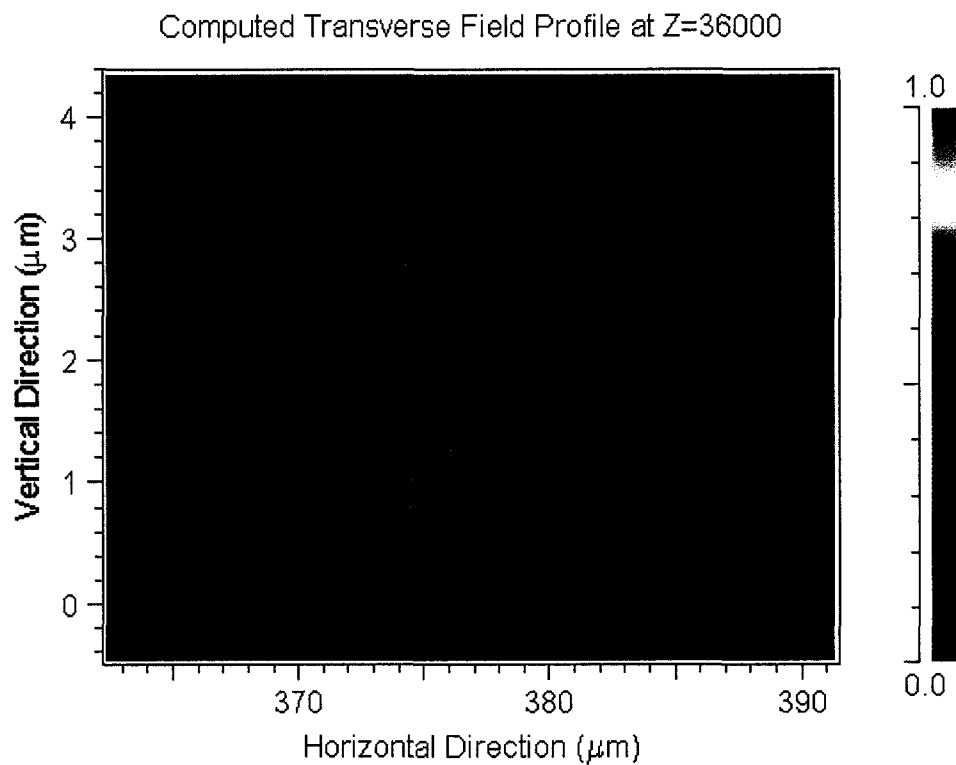


Figure 3.4: Transverse field profile of a rib waveguide ($W=4 \mu\text{m}$) at $z=36000 \mu\text{m}$

Even though the single-mode conditions for rib waveguides were applied, the question remains as to whether the high order modes will be cut off as expected. In order to solve this issue, BeamPROP, a commercial software package which uses FD-BPM in its calculation, was exploited.

To verify the single-mode behavior of the proposed rib waveguides, a method that Pogossian et al. [20] developed was applied. A gaussian beam was launched into these waveguides at $z=0 \mu\text{m}$ (Waveguide dimensions are as shown in Table 3.1, and the propagation distance in the guide is denoted as z). The transverse field profiles were then picked up at $z=36000 \mu\text{m}$. A plot of these transverse field profiles is shown in Figure 3.4. It can be clearly recognized that the shape of the field at $z=36000 \mu\text{m}$ is close to the fundamental mode of the rib waveguides with only one peak at the center region. Thus, it is proved that the proposed rib waveguides are effectively single-mode.

3.2 Strip-loaded shallow rib waveguides

The shape of the fundamental mode in a rib waveguide is strongly determined by the discontinuity along the edges of the rib. Basically, we expect the shape of the fundamental mode to be more like a Gaussian, so that more light can be coupled into the waveguide from an input fiber. The deeper the rib is, the closer the mode is to a Gaussian. However, experimental results presented in Chapter 4 show As_2Se_3 thin films do not have good adhesion and are subjected to high stress. Also, deep-etching these films through conventional wet or dry etching techniques has proven troublesome. Thus, a different method to fabricate large cross-section rib waveguides was required. Strip-loaded shallow rib waveguides were finally fabricated, and are analyzed in detail.

The structure of the proposed strip-loaded shallow rib waveguides is shown in Figure 3.5. After a BCB buffer layer was added to silicon wafer in order to improve adhesion, a TORLON strip is applied on top of the shallow rib. The strip

gives the waveguide lateral confinement, and the shallow rib further confines the light in the center region and reduces the mode loss [30].

Another reason that a strip was added on the rib is that the strip-loaded structure is easier to fabricate [31]. Mode loss was found to be strongly dependant on interface roughness in rib waveguides [32], while in these strip-loaded shallow rib waveguides, the requirement on the edge roughness of the strip is no longer as severe as in rib waveguides [32], since most of the light is confined in the film under the strip as shown in Section 3.2.2.

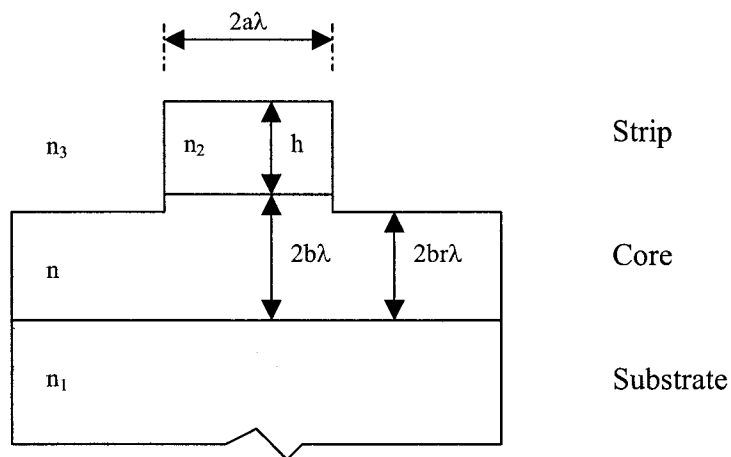


Figure 3.5: Scheme of strip-loaded shallow rib waveguide

3.2.1 Design of strip-loaded shallow rib waveguides

The strip-loaded shallow rib waveguide is a hybrid between a strip-loaded waveguide and a rib waveguide. It belongs to a class of waveguide called open dielectric waveguides [22] (slab-coupled waveguides in [19], rectangular dielectric waveguides in [25]). Open dielectric waveguides, especially rib waveguides have been analyzed in the literature using mode-matching techniques [21-29]. Among the articles, the result of Soref et al. [21] for rib waveguides have greatly been

discussed and quoted. Their result is given in a normalized form, and can be adapted for strip-loaded shallow rib waveguides.

In view of the fact that rib waveguides are strip-loaded rib waveguides with $n_2 = n_3$ (Figure 3.5), generalizing the single-mode conditions that Soref et al. derived for rib waveguides to strip-loaded shallow rib waveguides yields a relation between the transversal sizes of these waveguides for single mode propagation:

Defining the height of the rib as $2b\lambda$, and the height in the side regions (refer to Figure 3.5) are $2br\lambda$, when

$$r > 0.5, \quad (3.3)$$

Then higher-order modes in the vertical direction (EH_{10} , HE_{10} modes and the higher-order EH_{m0} , HE_{m0} modes) will be cut off [21]. The main underlying physical assumption of the above condition is based on the fact that when $r > 0.5$, the effective index of the fundamental slab mode in the side regions becomes higher than the effective index of any high-order vertical mode in the central region. The higher-order modes in the central rib section will be leaky and coupled to the fundamental mode in the side regions.

For $r > 0.5$, it was found by Soref et al. [21] that the EH_{01} , HE_{01} modes and the higher-order EH_{0m} , HE_{0m} modes will cease to propagate if

$$V < V_s \quad (3.4)$$

$$\text{where: } V = \frac{\pi}{2} \frac{aw_1}{b} \sqrt{\delta}, \quad (3.5)$$

$$V_s = \frac{\pi}{2} (1 + 0.3\sqrt{\delta}), \quad (3.6)$$

$$\text{and } w_1 = \frac{4\pi b}{q_1 + 4\pi b}, \quad (3.7)$$

$$\delta = \left(\frac{h_i}{h_o}\right)^2 - 1 = \left(\frac{w_2}{rw_1}\right)^2 - 1 = \left[\frac{q_1 + 4\pi b}{q_2 + 4\pi rb}\right]^2 - 1 \quad (3.8)$$

$$\text{with } h_i = 2b\lambda/w_1, \quad (3.9)$$

$$h_o = 2br\lambda/w_2, \quad (3.10)$$

$$w_2 = \frac{4\pi rb}{q_2 + 4\pi rb}, \quad (3.11)$$

$$q_1 = \frac{\gamma_{c0}}{\sqrt{n^2 - n_2^2}} + \frac{\gamma_{c2}}{\sqrt{n^2 - n_1^2}}, \quad (3.12)$$

$$q_2 = \frac{\gamma_{s0}}{\sqrt{n^2 - n_0^2}} + \frac{\gamma_{s2}}{\sqrt{n^2 - n_1^2}}. \quad (3.13)$$

n, n_1, n_2, n_3 are the refractive indices of the core, lower cladding, strip and the upper cladding respectively (see Figure 3.5 for detail). For TE modes, $\gamma_{c0}, c_2, s_0, s_2 = 1$; for TM modes, $\gamma_{c0}, c_2 = (n_{2,1}/n)^2$, $\gamma_{s0}, s_2 = (n_{3,1}/n)^2$. $2a\gamma$ and h_2 are the width and the height of the strip respectively as shown in Figure 3.5.

Substituting (3.5) and (3.6) into equation (3.4) yields

$$\frac{a}{b} < \frac{1}{w_1} \left(0.3 + \frac{1}{\sqrt{\delta}}\right). \quad (3.14)$$

Coding the conditions (3.3) and (3.14) for strip-loaded shallow rib waveguides in Matlab generated the following plot for the height of the rib = 1 μm . As shown in this plot, when etching depth increases, both rib and strip-loaded shallow rib waveguide width must decrease to maintain only single-mode operation. At some point, this width may be too narrow for fabrication and/or introduce unacceptable coupling loss. Compared to rib waveguides, strip-loaded

shallow rib waveguides allow a wider rib for the same etching depth in most cases, and thus are easier to fabricate.

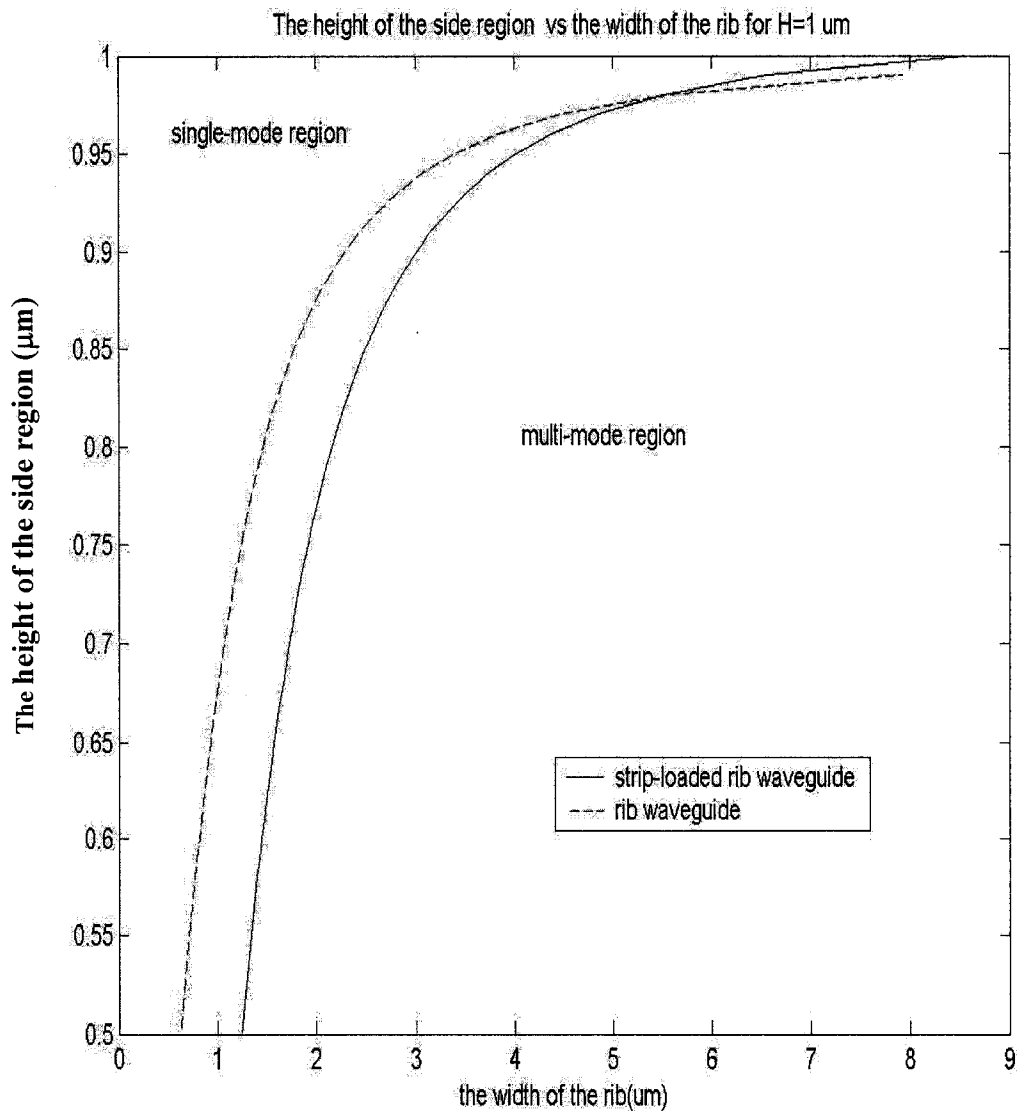


Figure 3.6: Single-mode condition curve for strip-loaded shallow rib waveguide

Based on the curve in Figure 3.6, the following single-mode strip-loaded shallow rib waveguides were finally fabricated [H: the height of the rib region, h: the height of the outside region, W: the width of the rib].

Waveguide No.	S-1	S-2	S-3	S-4	S-5	S-6	S-7	S-8
W (μm)	3.0	2.9	2.8	2.7	2.6	2.5	2.4	2.3
H (μm)	1	1	1	1	1	1	1	1
h (μm)	0.9	0.9	0.9	0.9	0.9	0.9	0.9	0.9
Length (cm)	3	3	3	3	3	3	3	3

Table 3.2: Fabricated strip-loaded shallow rib waveguide dimensions

The above dimensions were crosschecked with Marcatili method [19] to ensure that the proposed strip-loaded shallow rib waveguides are mono-mode. As indicated by Marcatili, the penetration depth of higher-order modes can be infinite due to well-defined proportional sizes of the height and the width in the central region. When propagating, high-order modes will be filtered out by coupling to radiation modes. The number of modes, N , of a slab-coupled guide is mostly determined by its geometry. Following Ref. [19],

$$N = \frac{\pi WH}{4 T^2} \quad (3.15)$$

$$\text{where: } T = 2br\lambda(1 + c_t), \quad (3.16)$$

$$W = 2a\lambda(1 + c_w), \quad (3.17)$$

$$H = 2b\lambda(1 + c_h), \quad (3.18)$$

$$v_{1,2,3} = kh\sqrt{n^2 - n_{1,2,3}^2}, \quad (3.19)$$

$$c_t = \frac{1}{r} \left(\frac{1}{v_1} + \frac{1}{v_3} \right), \quad (3.20)$$

$$c_h = \frac{1}{v_1} + \frac{1}{v_2} \tanh\left(\frac{h_2}{h} v_2 + \tanh^{-1} \frac{v_2}{v_3}\right), \quad (3.21)$$

$$\text{and } c_w = \frac{2b}{av_3} \frac{n_3^2}{n^2}. \quad (3.22)$$

Our calculation with the Marcatili method proves all the fabricated strip-loaded shallow rib waveguides are single-mode ($N < 2$).

3.2.2 Simulation of strip-loaded shallow rib waveguides

The commercial software package tempSelene was used to derive the fundamental mode profiles for the proposed strip-loaded shallow rib waveguides. In view of the fact that the etching depth is hard to control during the processing of As_2Se_3 , the effective index method was coded in Matlab in order to derive the confinement changes in terms of etching depth (See Appendix IV).

1) Effective indices

Waveguide No.	S-1	S-2	S-3	S-4	S-5	S-6	S-7	S-8
Width(um)	3.0	2.9	2.8	2.7	2.6	2.5	2.4	2.3
Neffrib	2.6455	2.6455	2.6455	2.6455	2.6455	2.6455	2.6455	2.6455
Neffout	2.6295	2.6295	2.6295	2.6295	2.6295	2.6295	2.6295	2.6295
Neff	2.6406	2.6404	2.6401	2.6399	2.6397	2.6394	2.6391	2.6389

Table 3.3: Effective indices of the proposed strip-loaded shallow rib waveguides

The lateral confinement in an open dielectric waveguide is greatly defined by the modal refractive index or the refractive index offset between the center region and the side regions, and can be analyzed by the effective index method. Coding the effective index method in Matlab resulted in Table 3.3 and Figure 3.7.

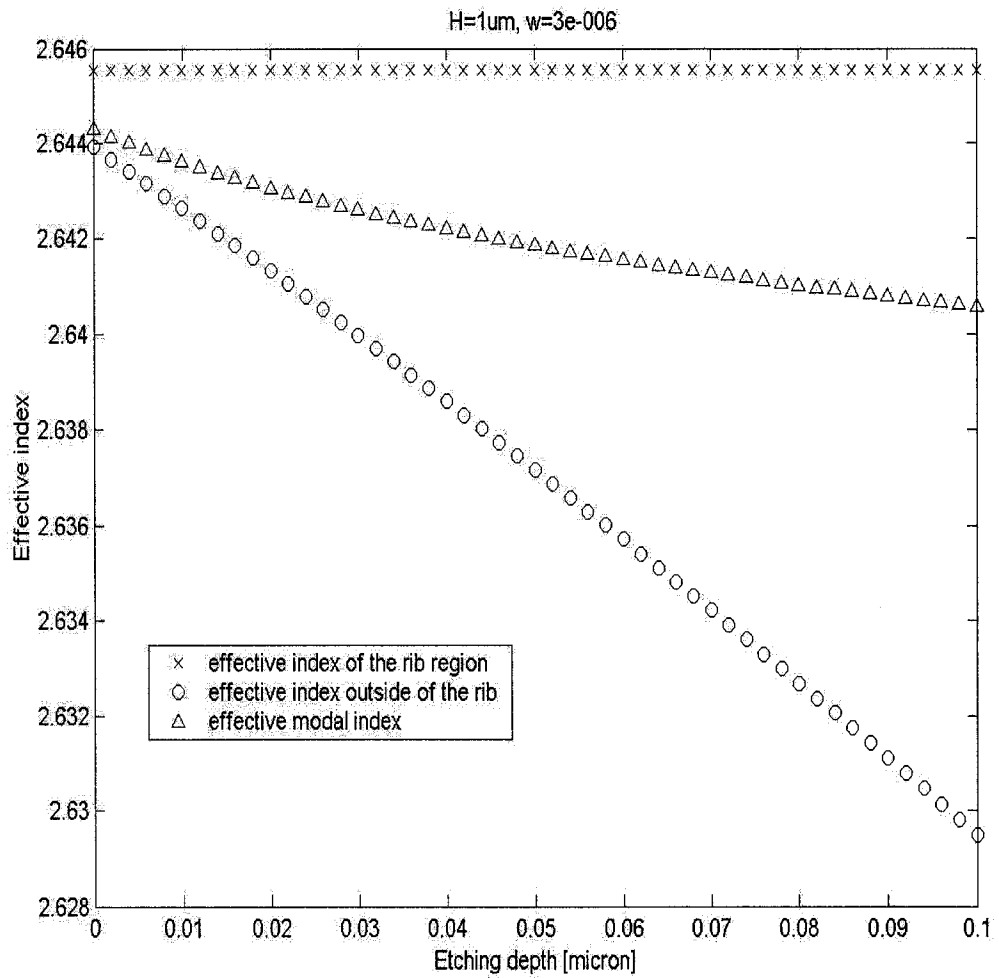


Figure 3.7: Effective index vs. etching depth

As seen from Table 3.3, when the width of the rib decreases, the effective index of the fundamental mode decreases, resulting in greater field penetration in the side regions. On the contrast, when the width of the rib increases, the effective index of the fundamental mode increases, resulting in a strong confinement in the lateral direction.

While Table 3.3 shows the effective index changes with the width of the rib, Figure 3.7 demonstrates the index offset between the rib region and side regions increases with etching depth in strip-loaded shallow rib waveguides, resulting a stronger confinement. This can be interpreted using the ray optics. As etching depth increases, the lateral ‘glancing’ bounce angle of the fundamental mode increases, thus has a higher percentage of its field under the rib.

The lateral confinement is related to many properties of the waveguide, such as waveguide density in an integrated optical circuit and allowable bend radius. As deep etching is difficult for As_2Se_3 film, the proposed waveguides do not have a strong lateral confinement. Thus, the bend radii cannot be too small as discussed in Chapter 2.

2. Fundamental mode profiles

The fundamental mode profiles were derived by running the Mode Cal in tempSelene. Finite difference method was used with H, h and W as illustrated in Table 3.2, $n_{\text{core}}=2.72$, $n_{\text{strip}}=1.54$, $n_{\text{up}}=1$, $n_{\text{down}}=1.62$, strip thickness=1 μm , substrate thickness=10 μm , and calculation window was defined as 50 μm X 50 μm . The resulting figure (Figure 3.8) shows strip-loaded shallow rib waveguides have better mode shape in terms of coupling light from a single mode fiber for the reason that compared to strip-loaded waveguides and rib waveguides, the fundamental mode profiles of the proposed strip-loaded rib waveguides are more circular with most of the energy (80%) is confined under the rib (shown by the red circle).

In the case of strip-loaded waveguides, the fundamental modes spread a lot to the sides, thus the waveguides should be further apart. A rib, even a shallow one, can help to further confine light in the center region. The deeper the rib is, the better the light is confined. This is consistent with what we get from the EI method.

Replacing the strip with a higher refractive index material, such as As_2S_3 (refractive index ~ 2.5) or Ga:La:S glasses, can improve the coupling coefficient as well, because the mode shape will have better match with the output of single-mode fibers.

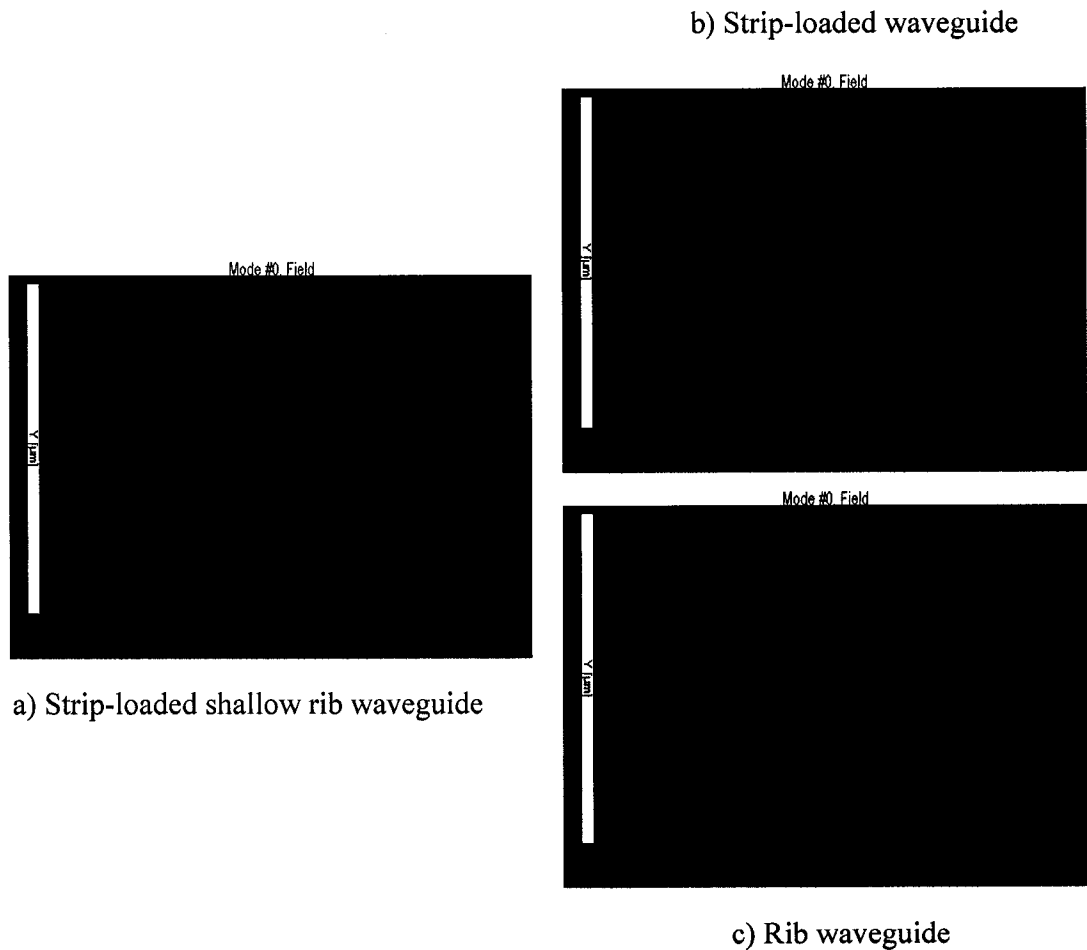
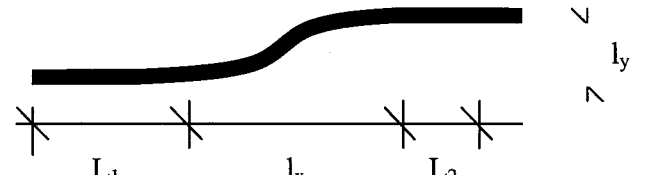


Figure 3.8: Fundamental mode profiles

3.3 Bends and splitters

3.3.1 Design of sine-bends and Y-splitters

Sine-bend No.	S-1	S-2	S-3	S-4	S-5	S-6
l_x (cm)	4.0	4.0	4.0	4.0	4.0	4.0
l_y (μm)	125	250	375	125	250	375
W (μm)	2.5			2.3		
H (μm)	1			1		
h (μm)	0.9			0.9		
L_1 (cm)	0.05					
L_2 (cm)	0.45					



Remark: $L_{1,2}$ and l_x are the length of the added straight sections and bend section respectively.

Table 3.4: Fabricated sine-bend (refer to equation 2.1) dimensions

Sine-wave s-bends were used for the bends and Y-splitters in this project since it minimizes the bending loss discussed in Chapter 2. The length of the bends should be not less than 100 times of the offset in the transverse direction, because there is no tight horizontal confinement. The separation between two nearby

outputs in bend sections is a multiple of $125 \mu\text{m}$ as it is the standard of integrated optics. Two straight sections are added before and after the bend section in order to observe the light changes in the curved area during testing.

The fabricated sine-bends are shown in Table 3.4, while the fabricated Y-splitters are illustrated in Table 3.5.

Y-splitter No.	Y-1	Y-2	Y-3	Y-4	Y-5	Y-6
l_x (cm)	4.0	4.0	4.0	4.0	4.0	4.0
l_y (μm)	250	500	750	250	500	750
W (μm)	4.0			3.8		
H (μm)	1			1		
h (μm)	0.9			0.9		
L_1 (cm)	0.05					
L_2 (cm)	0.45					

Remark: $L_{1,2}$ and l_x are the length of the added straight sections and branch section respectively.

Table 3.5: Fabricated Y-splitter dimensions

3.3.2 Simulation of sine-bends and Y-splitters

The energy flow along the propagation direction gives us a clear picture of how the light evolves in the proposed sine-bends and Y-splitters, and can be simulated with BeamPROP, a simulation program using finite-difference beam propagation techniques.

Running BeamPROP generates the following plot (Figure 3.9) for a sine-bend. As seen from this graph, when light goes through a sine-bend, it will lose part of its energy. This can be explained as the power is coupled from fundamental mode to radiation modes. As calculated by BeamPROP, losses are around 30% for our proposed sine-bends.

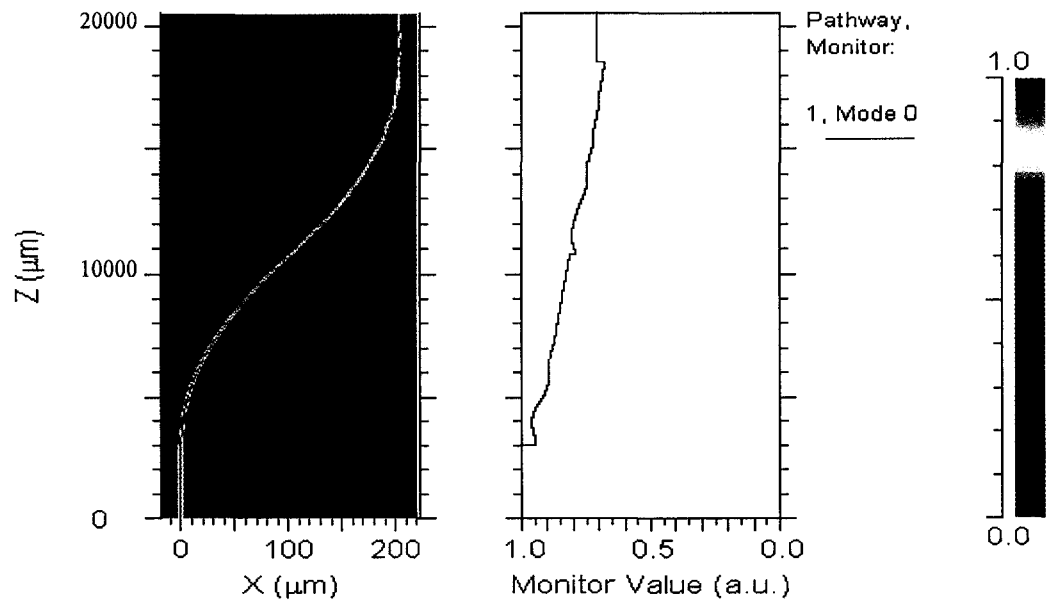


Figure 3.9: Beam propagating in a sine-bend (refer to equation 2.1)

Note: Monitor value is the light power propagating under the strip (see Figure 3.1).

3.4 Mask design

A prototype mask was designed for optical lithography of the waveguide structures. Quartz was used as the substrate, and chromium is applied as the opaque layer. Thus, the mask is more robust and will not wear out in a short time.

The waveguides were defined by e-beam, and were arranged by its width and function as shown in Appendix VI. The waveguides are also labeled to facilitate identifications during inspection. Alignment marks were included in order to provide angular alignment during exposure.

4. Waveguide fabrication

Fabrication is the key step in this project. Whether the waveguides are feasible depends on the fabrication techniques, as well as the materials. In this chapter, the fabrication and experimental results of the proposed inverted rib waveguides will be discussed. Also, the fabrication recipe of the proposed strip-loaded shallow rib waveguides will be described in detail.

4.1 Inverted rib waveguide fabrication

Inverted rib waveguides are initially proposed, as the rib channels can be constructed by silicon dioxide etching, which is well known.

4.1.1 Fabrication processes

The steps [Figure 4.1] required for making the proposed As_2Se_3 inverted rib waveguides are:

a) Wafer preparation

Commercial silica wafers (orientation: $\langle 100 \rangle$, diameter: 5", silicon dioxide thickness: 2 μm) are applied as the substrates for the proposed As_2Se_3 inverted rib waveguides.

The silica substrates are cleaned using a "piranha" solution (1800 ml sulfuric acid and 600 ml hydrogen peroxide, see Appendix VII for recipe). Cleaning is necessary for the subsequent processes, as not all the material adhere well to oxides, and adhesion is generally improved on clean surfaces.

b) Chrome sputtering

One layer of chrome is sputtered on top of silica wafers. This layer of chrome will work as the etching mask for transferring the waveguide pattern onto the surface of the silica wafers later. Chrome is chosen because most of the other metals, as well as photoresist are etched by CHF_3 , the etchant for silicon dioxide in RIE.

Lesken sputtering system is used in this project for chrome deposition, as sputtering has advantages over evaporation. The sputtering system pressure is maintained at 1.3×10^{-6} torr so that it can provide fairly good coverage, and films have higher density and larger grain.

c) Photolithography

In this step, the pattern on the prototype mask is transferred to a layer of positive photoresist which is then the mask for the chrome etching (For detail lithography recipe, please refer to Appendix VII).

Pre-dehydration baking of the substrates at 200°C is necessary for positive PR, as positive PR doesn't always adhere well. PR is then applied to the wafers by spinning. The thickness of the PR is determined by the spinning speed, as well as the viscosity and acceleration. In the proposed inverted rib waveguide fabrication, the spinning is set at 4000rpm for 40s.

To drive off the extra solvent, the wafers with PR on top are baked before exposure at 115°C for 90s on a hot plate. PR is exposed to UV light for 4s and developed in Developer 354 solution for 15s afterward.

d) Chrome etching and PR stripping off

This step is to define the proposed pattern on the chrome layer which is then the mask for silica etching.

In this step, wafers are simply dipped into cerium ammonium nitrated solution which preferentially remove chrome without substantially degrading the PR pattern. After chrome etching, the remaining positive photoresist is then stripped off in acetone.

e) Silicon dioxide etching and chrome stripping

This step implements the proposed rib channel in silicon dioxide using reactive ion etching.

CFH_3 is used as the precursor gas for RIE, as this gas will be broken down into sub-fluorides CF_x , which then can etch silica. The gas flow rate is 20 sccm, while the RF power is set to be 150W and cubical pressure 45 mtorr.

As the major advantage of plasma etching is the possibility of anisotropic etching due to ion bombardment, a lower pressure and a higher RF power increase ion energy, thus cause more vertical sidewalls and relatively less undercutting. However, they can also cause lower etching rater and rough surface.

Chrome is stripped off after silica etching using cerium ammonium nitrated solution.

f) As_2Se_3 bulk material preparation and As_2Se_3 evaporation

This step is to deposit As_2Se_3 on top of silica and construct the desired rib waveguides.

In this process, As_2Se_3 bulk material is first prepared by melt quenching. Melt quenching is a way to prepare bulk glasses by rapidly cooling (quenching) the liquid

materials. Whether the material will crystallize or form a glass upon cooling mainly depends on the temperature of the oven and the rate of cooling. As_2Se_3 is good glass formers, which means it can be made amorphous easily without extreme conditions, such as an extra high cooling rate.

As_2Se_3 bulk material is then place in an evaporator, and As_2Se_3 thin films are prepared by vapor deposition. The chamber pressure is controlled at 2×10^{-6} Torr, while the evaporation power is $7\text{V} \times 145\text{A}$. The substrate is rotated, so that the produced thin films will be as homogeneous as possible, with uniform thickness.

Similar to the cooling rate in melt quenching, the parameter in vapor deposition is the deposition rate. The faster the film is deposited, the more “amorphous” it is. Evaporation works well on As_2Se_3 . Being a good glass former, As_2Se_3 thin films usually do not require a particular deposition rate (10nm/s in our case). Moreover, As_2Se_3 has a glass transition temperature (T_g) as low as 468K, which is attractive for evaporation.

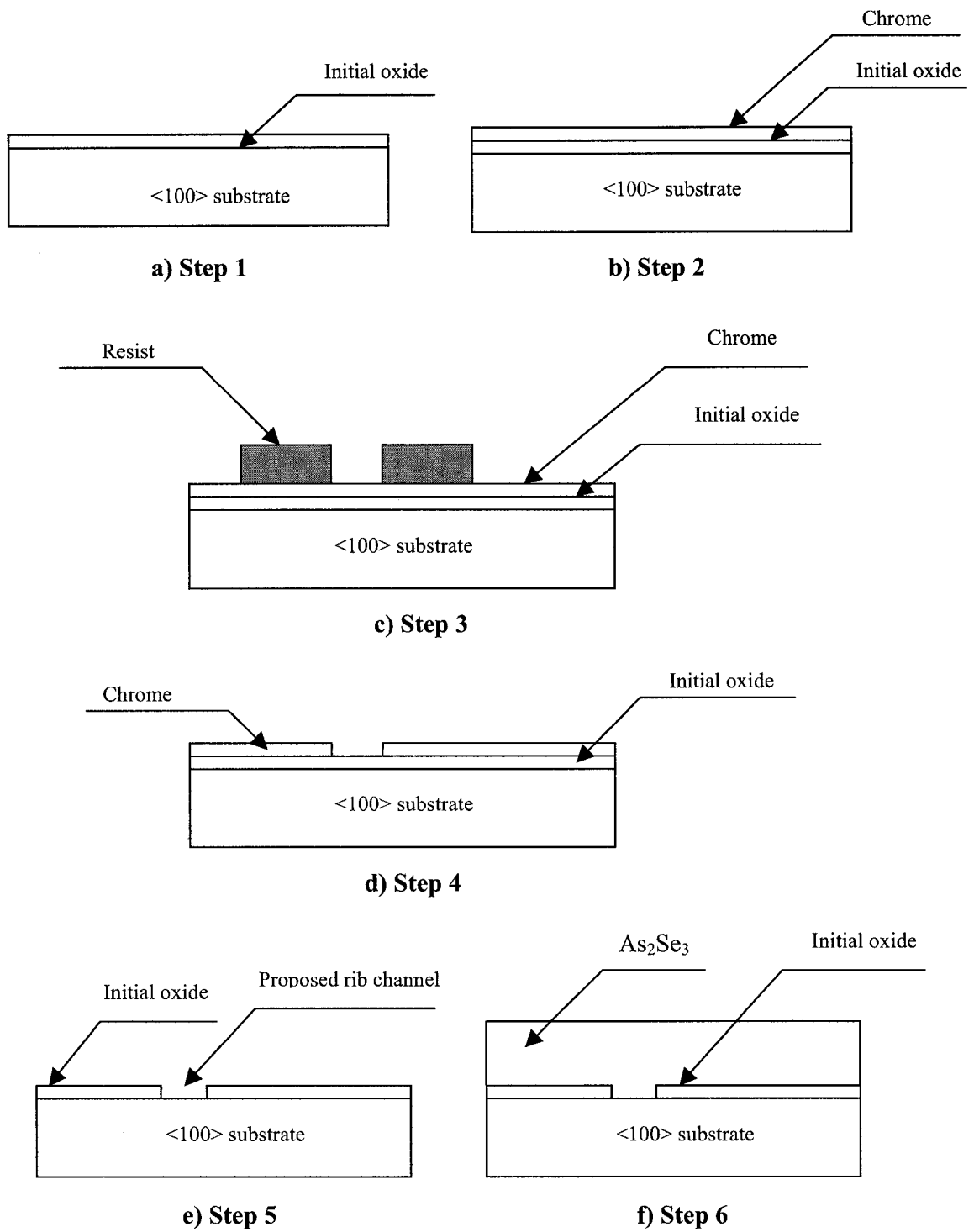


Figure 4.1: Inverted rib waveguide fabrication receipt

4.1.2 Obstacles in fabrication

The proposed inverted rib waveguides cannot be fabricated as expected. The problems, which are related to the materials, are analyzed as followed:

1) As_2Se_3 films do not stick to SiO_2 wafer very well due to different bond lengths and angles. Different buffer materials (TORLON, BCB) and different treatments, e.g. hexamethyldisilazane (HDMS), annealing, were tried to improve the adhesion. It seems TORLON and BCB have better adhesion than SiO_2 . HDMS does not work on As_2Se_3 films.

2) CHG (As_2Se_3) films suffer from high stress due to different thermal expansion coefficient (SiO_2 : 0.5 ppm/ $^\circ\text{C}$, BCB: 52 ppm/ $^\circ\text{C}$, As_2Se_3 : 21 ppm/ $^\circ\text{C}$) from the underlying layer. Thus, the adhesion problem is compounded.

It is said in the literature that annealing can help to relieve residual stress and minimize the scattering losses of the guided wave [5]. However, research at TRILabs has shown that As_2Se_3 films with SiO_2 or BCB as under-cladding become more fragile after annealing at different temperature range from 30 $^\circ\text{C}$ to 170 $^\circ\text{C}$ (the glass-transition temperature T_g). Different annealing temperatures with different durations have been tried. The reason for this is still unknown.

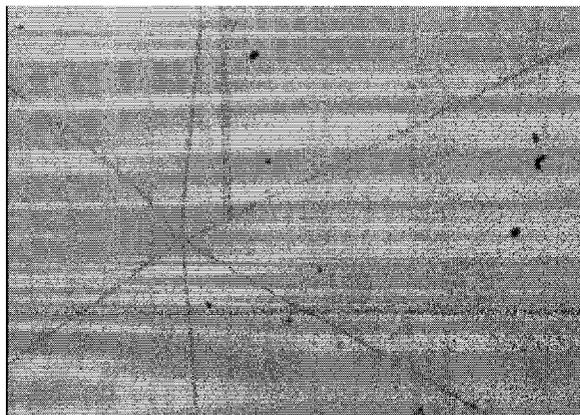


Figure 4.2: Stress cracks a sample which had been sitting for 12 days

3) CHG (As_2Se_3) films have shown degradation over time.

For example, stress cracks may show up in a film which has been sitting outside clean room for seven days [Figure 4.1]. Apparently, the glass structure cannot stand the stress with time.

4) Basically, all alkaline solutions can etch As_2Se_3 .

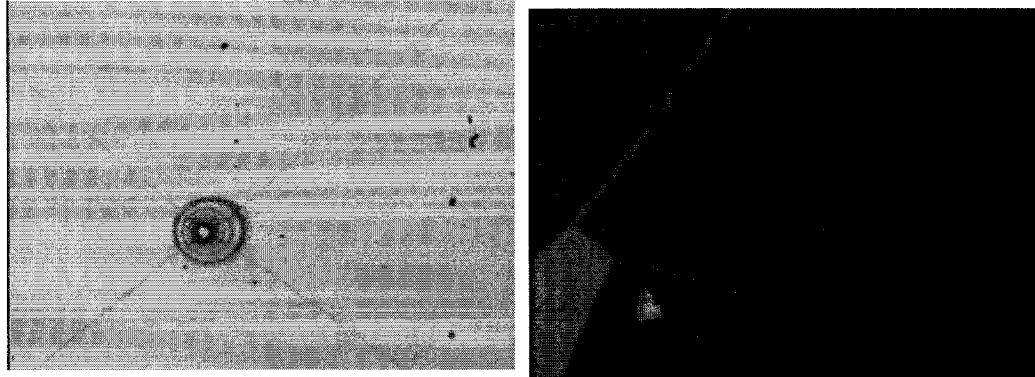
Monoethanolamine (MEA), ethylenediamine (EDA), NaOH and NH_4OH have been intensively tested to determine etching rates and etching conditions. EDA and NaOH are very active. Fumes are generated and As_2Se_3 film will peel off after several tens of seconds. MEA and NH_4OH have better controllability. For MEA, the solvent can be heated up to increase etching rate.

An etching rate of 200nm per minute was measured for MEA which has been heated up to 45°C, and 20nm per minute for NH_4OH at room temperature.

5) Lithography might be difficult because most of the PR developers (NaOH for positive photoresist and NH_4OH for negative resist normally) available in Microfab are alkaline solutions.

6) Due to the chemical and adhesion characteristics of As_2Se_3 films, etching depths can only reach several hundred nanometer. If the film submerges in the etchants for a longer time, the solvents will go underneath through defects [Figure 4.2 (a)] and later the film will peel off [Figure 4.2 (b)].

Our final experimental result showed that etching 100-200 nm is easier to achieve, and it is more repeatable.



a) Solvents go underneath

b) As₂Se₃ film peels off

Figure 4.3: Deep-etching problem of As₂Se₃ film

7) For As₂Se₃, evaporation does not provide good sidewall coverage [Figure 4.3].

SEM shows the step coverage, which is defined as the ratio of minimum sidewall coverage to the normal film thickness on the top surface, is around 3.21%. This means evaporation has poor ability to deposit film uniformly over topographical features.

Unless the substrate is also very hot, the As₂Se₃ molecules most probably will stick to the surface each time they strike. The sticking coefficient is very close to one, thus the As₂Se₃ cannot fill the rib channel as expected. The shape of the fabricated inverted rib waveguides is not as nice as in Figure 3.1, as seams appear along the rib channels (shown in Figure 4.3), and bubbles and ripples distort the waveguide structure.

Poor sidewall coverage, as well as the columnar structure due to the angular distribution of flux, are typical problems of evaporation. In addition to heating the wafer in evaporation, sputtering will provide better sidewall coverage. However, the availability in Microfab (no suitable sputtering system for As₂Se₃) limits our choice in experiment.

Because perturbations, e.g. seams, bubbles and ripples, are the reason for a high level loss in waveguides, the proposed inverted rib waveguides are not feasible.

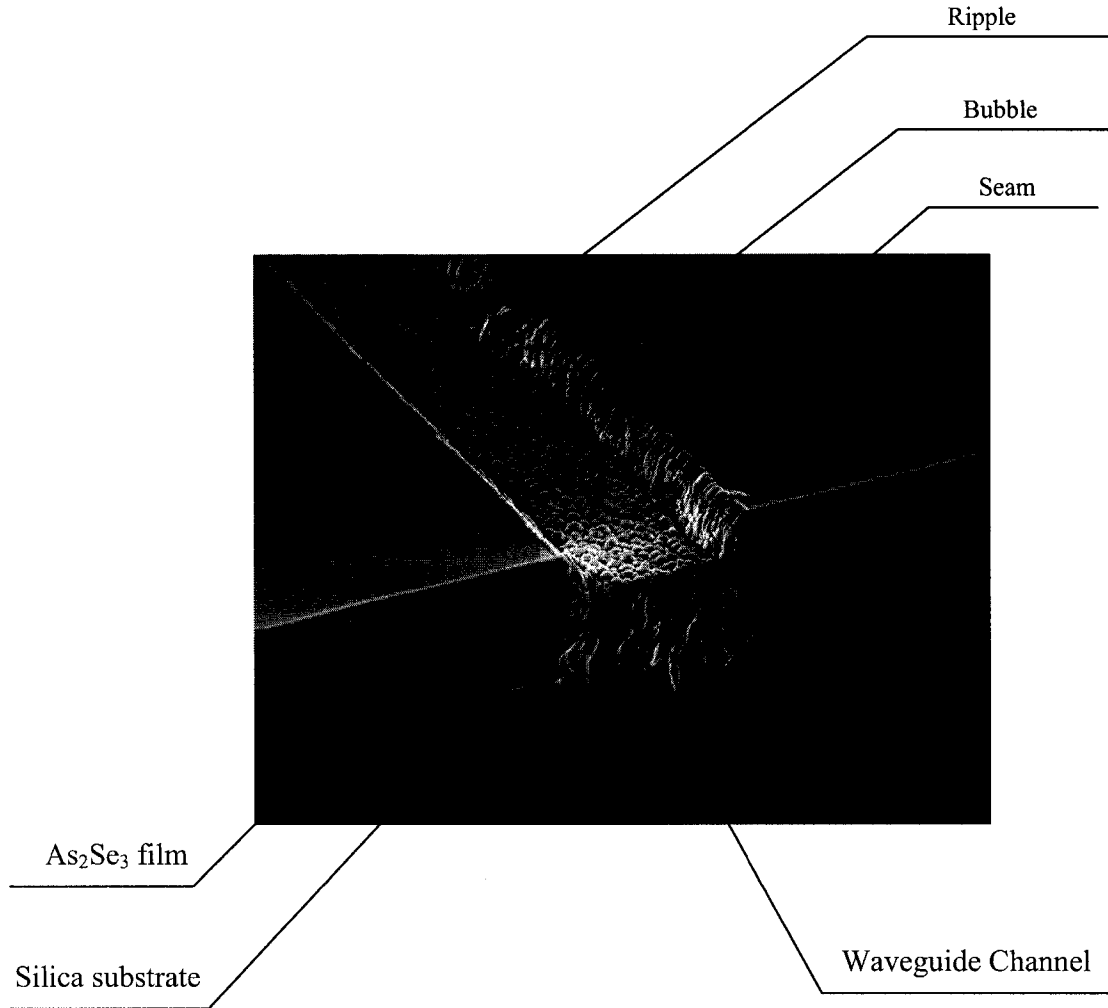


Figure 4.4: SEM picture of a fabricated inverted rib waveguide

4.2 Strip-loaded shallow rib waveguide fabrication

As discovered in the fabrication of the inverted rib waveguides, deep etching is impossible, and large cross-section rib waveguides need to be modified. Based on the characteristics of As_2Se_3 thin films, strip-loaded shallow rib waveguides were proposed,

as these structures do not require deep etching, have a simple fabrication procedure and relatively good optical properties.

4.2.1 Fabrication processes

The fabrication of the proposed As_2Se_3 strip-loaded shallow rib waveguides involves the following steps.

a) Wafer preparation

Commercial silicon wafers (orientation: $\langle 100 \rangle$, diameter: 5") are used as the substrates for the proposed As_2Se_3 strip-loaded shallow rib waveguides, and a BCB buffer layer will be applied on top of silicon to increase adhesion and provide total internal reflection.

The silicon substrates are cleaned using a "piranha" solution (see Appendix VII for recipe). Rigorous cleaning is necessary before BCB deposition, as dust generates pinholes in the BCB films.

b) BCB deposition

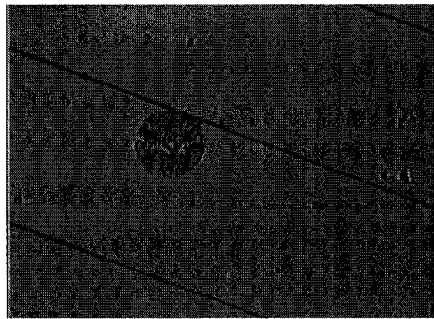
In this step, a BCB layer is deposited on top of silicon wafers by spinning to solve the problem of adhesion of the As_2Se_3 films.

The wafers are coated with Dow adhesion promoter AP3000 first, as BCB doesn't always adhere well. 20ml of BCB is then dispensed on the wafers and spun at 3000rpm for 30s. At last, T1100 ancillary chemical solvents are added at the edge of the wafers to remove the edge bead, and the substrates are cured in vacuum oven for one hour at 250C. The resulting films are approximately 10 microns thick.

c) As_2Se_3 bulk material preparation and As_2Se_3 evaporation

In this step, As_2Se_3 thin films are deposited as in inverted rib waveguide fabrication.

However, because As_2Se_3 doesn't always adhere well to BCB, cleaning becomes more critical. As been found out in process, cleaning the evaporator chamber every time before evaporation can greatly reduce pinhole and defect. Reducing pinhole and defect will prevent solvents from going underneath and peeling off the film in the coming processes.



a) Without cleaning



b) With cleaning

Figure 4.5: Clean-up can reduce pinhole and defect

d) TORLON deposition

Similar to BCB deposition, a layer of TORLON is deposited on top of As_2Se_3 by spinning. The wafers are first coated with TORLON at a very low speed, and then spun at 7000 rpm for 30s. The final TORLON thickness is around 1.2 microns (refer to Appendix VII for detail).

e) Photolithography

This step is to transfer the pattern on the prototype mask to a layer of negative photoresist which is then the mask for the TORLON etching and As_2Se_3 etching (see Appendix VII for recipe). Negative PR 5214 is used because the same mask for the inverted rib waveguides is applied. Similarly, MF321 is used as developer. Since the negative PR works as the mask for two consecutive etchings, the PR layer needs to be thicker. The spinning speed is thus lowered to 3500 rpm for 40s. The resulting thickness is approximately 2 μm .

f) TORLON Etching

This step implements the strip structure in TORLON for the proposed strip-loaded shallow rib waveguides using reactive ion etching.

O_2 (flow rate: 80sccm) and SF_6 (flow rate: 2.6sccm) are used as the precursor gases for RIE. While the RF power is set to be 150W, the chamber pressure is 93 mtorr.

g) As_2Se_3 etching

This step implements the shallow rib in As_2Se_3 for the proposed strip-loaded shallow rib waveguides using wet etching. The wafers are simply dipped into ammonium hydroxide solution for 5 minutes, and the As_2Se_3 layer will be etched down 100nm.

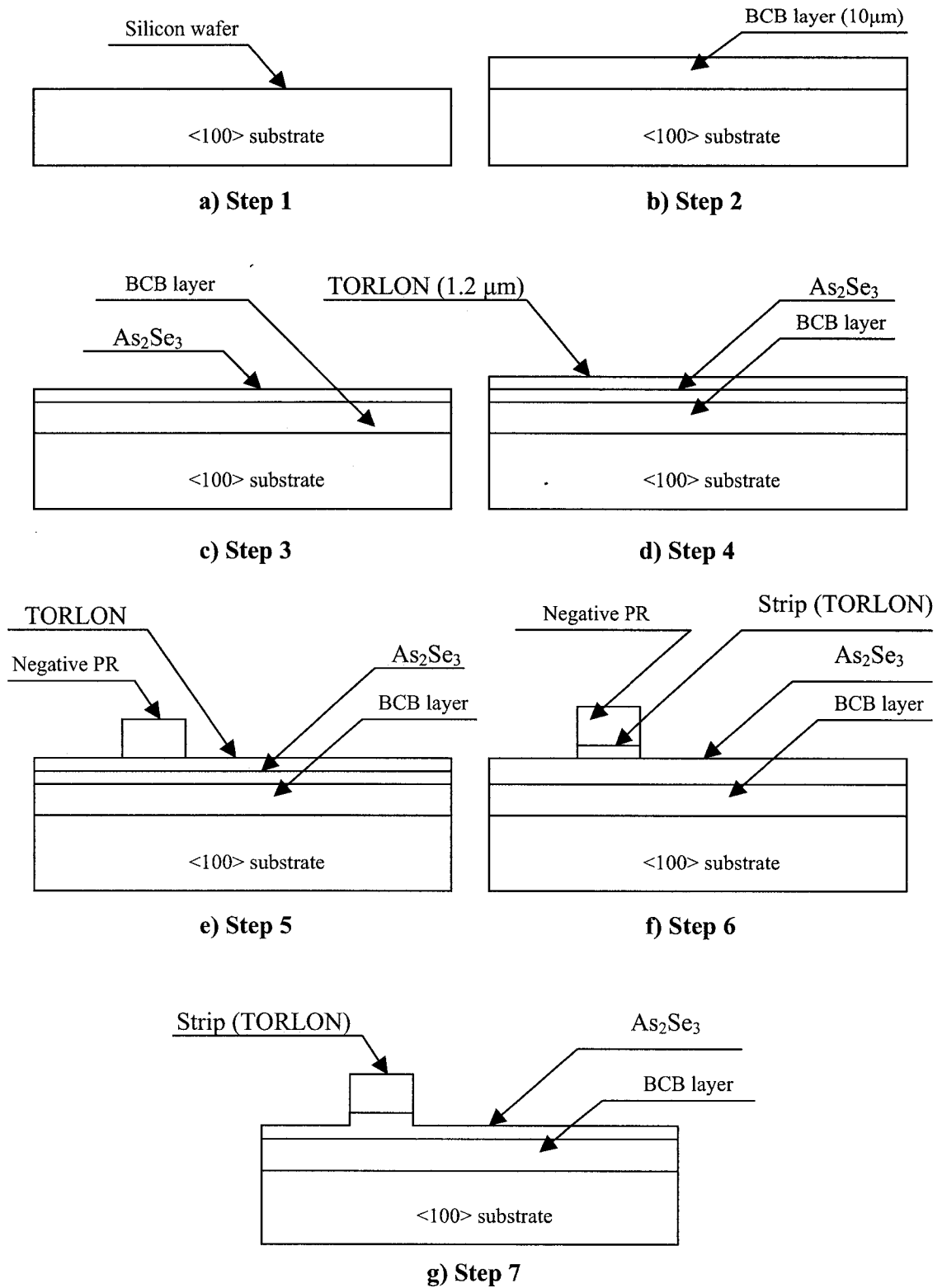


Figure 4.6: Strip-loaded shallow rib waveguide fabrication receipt

4.2.2 Discussion

Even though the shapes and dimensions of the strip-loaded shallow rib waveguides (shown in Figure 4.4) are generally as expected, there are still some issues that need to be analyzed.

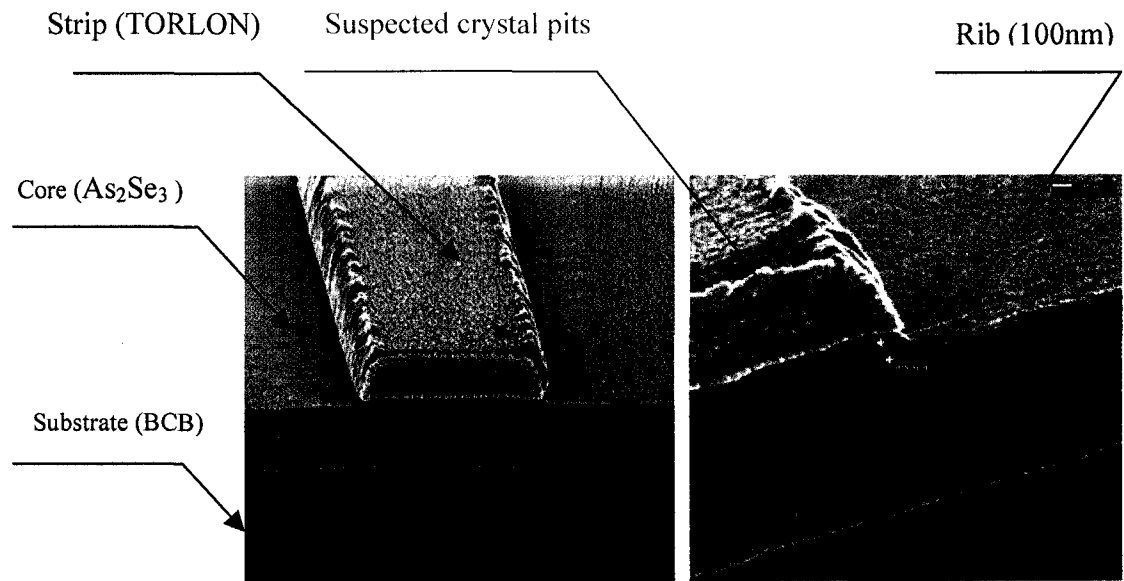


Figure 4.7: SEM pictures of a fabricated strip-loaded shallow rib waveguide

1. Negative PR is not thick enough to be the mask for both TORLON etching (Step f) and As₂Se₃ etching (Step g). As shown in Figure 4.7, the negative PR layer has gone in Step f, and the TORLON layer has been etched down as well.

Moreover, Ammonium hydroxide also reacts with TORLON slowly in step g, which result in the shrinking of strip (TORLON) both in vertical and horizontal direction.

Thus, the fabricated strip-loaded shallow rib waveguides will be smaller than the features on the mask, e.g. if the width of the feature on the mask is $3.8\ \mu\text{m}$, the fabricated strip-loaded shallow rib waveguide will only be $3.0\ \mu\text{m}$ wide.

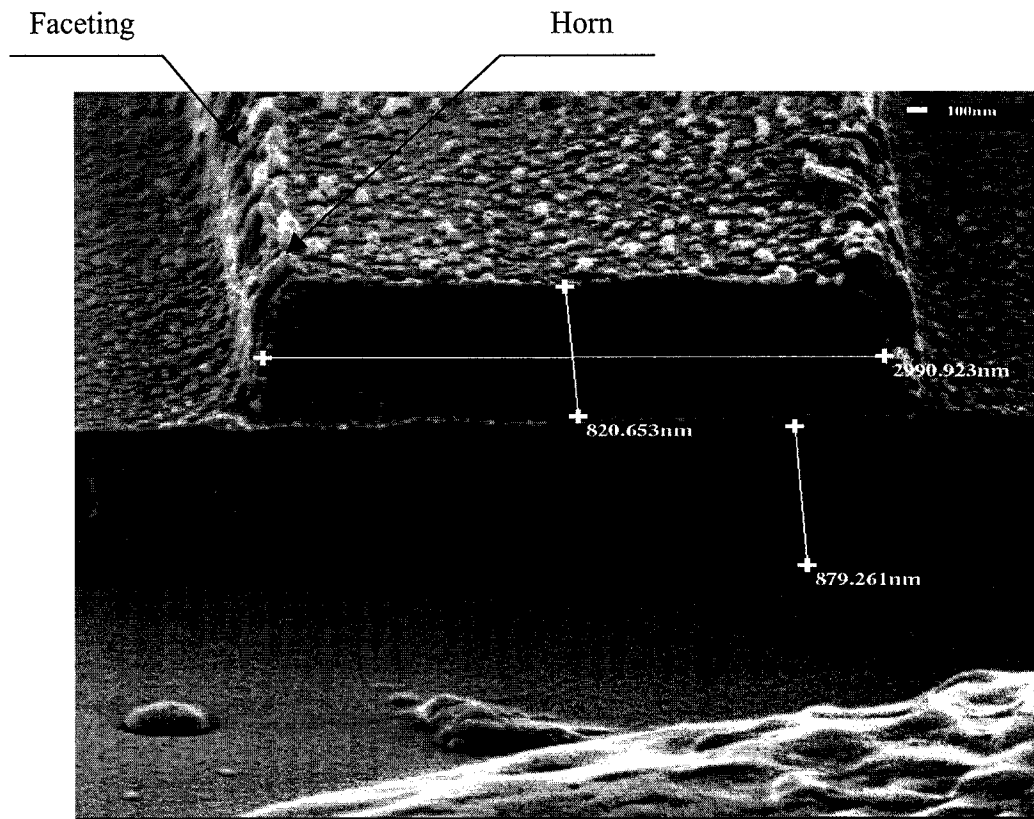


Figure 4.8: Sample structure after TORLON etching

2. In TORLON RIE (Step f), re-deposition on the sidewalls creates ‘horns’, and angular dependence of sputter yield causes faceting (see Figure 4.9), thus the fabricated strip-loaded shallow rib waveguides are not rectangular, and have a rough sidewall.

However, as discussed before, since most of the power is confined under the strip in strip-loaded shallow rib waveguides, surface roughness is no longer as important as in rib waveguides, so it is a minor issue.

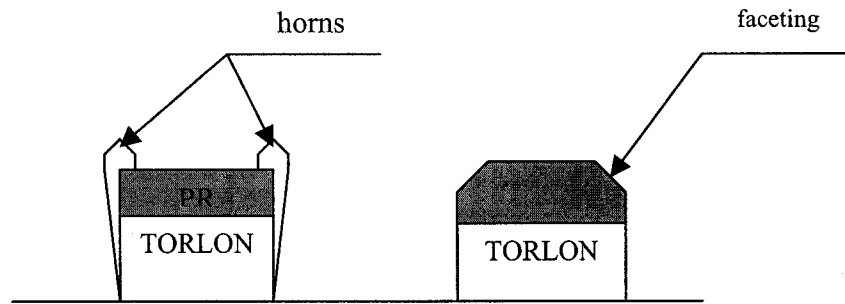


Figure 4.9: Horns and faceting in RIE

3. The As_2Se_3 films are suspected to undergo local crystallization in processes (most probably in baking). Crystal structure (see Figure 4.7) is observed in waveguide samples. The reason for this is still unknown. As discussed in Section 2.4, pits generated by crystallization can cause high loss in waveguide.

5. Waveguide testing

This chapter deals with the characterization of the As_2Se_3 strip-loaded shallow rib waveguides.

Even though the proposed strip-loaded shallow rib waveguides are designed for 1550 nm, calculation shows they also support single-mode propagation at wavelength of 980 nm. It is generally understood that for propagation at $\lambda=980$ nm, the mode size will be smaller, the propagation loss will be higher as Rayleigh scattering loss is proportional to $1/\lambda^4$ and the absorption coefficient also decreases with λ .

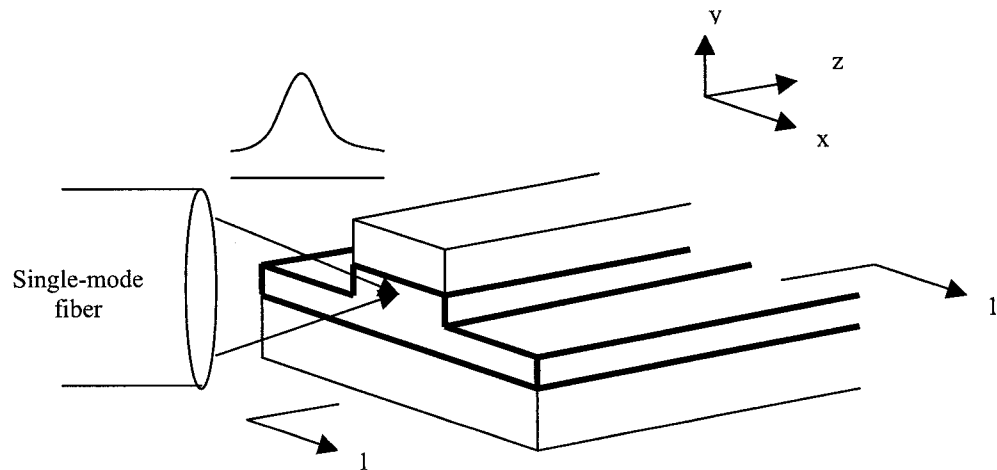


Figure 5.1: End coupling scheme

Light of wavelength 980 nm was end-coupled into waveguides from a single-mode fiber in testing as shown in Figure 5.1. The scattered light and waveguide output are captured by a camera, and the images were analyzed with the aid of a computer for the propagation losses and mode profiles. The waveguide testing was also tried for higher wavelengths such as 1310 nm and 1550 nm. However, without a proper camera, it is different to align the waveguides with the fiber.

5.1 Mode profile characterization

5.1.1 Mode profiles

The waveguide near-field patterns are imaged using the setup shown in Figure 2.11. The intensity distributions are derived with the help of IPLab, a software package. The intensity linear plots are shown in Figure 5.2 and Figure 5.3, while the output images are as shown in Figure 5.4.

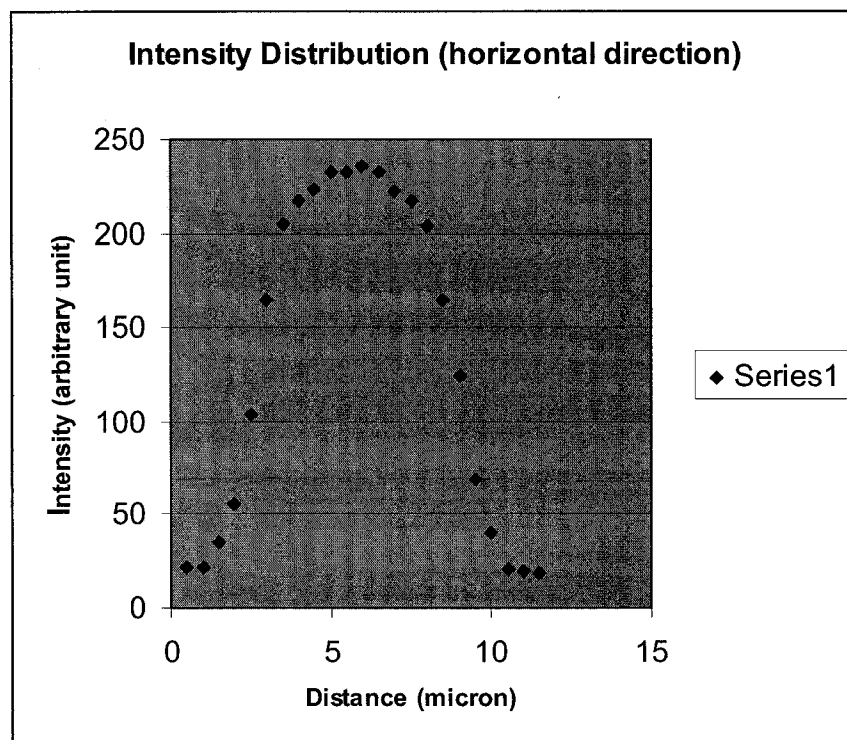


Figure 5.2: Intensity distribution of a waveguide output (horizontal direction)

Note: the distance is measured by comparing the output images to the film thickness that has been measured by profilometer.

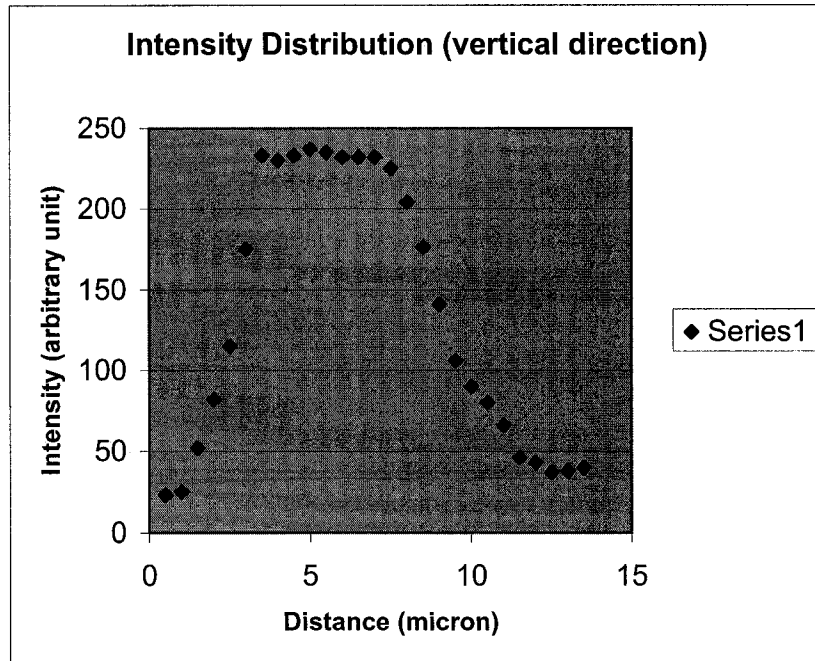
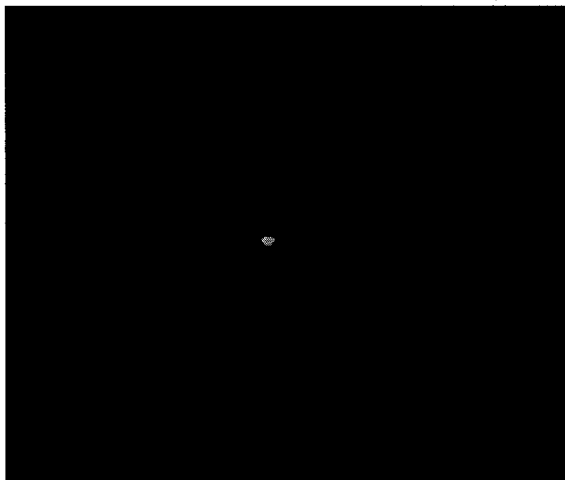
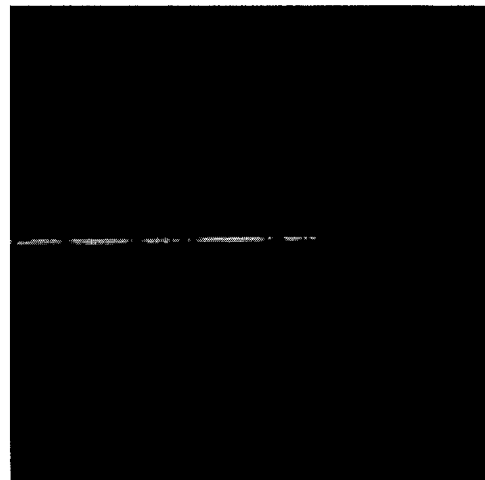


Figure 5.3: Intensity distribution of a waveguide output (vertical direction)



a) Rib region



b) Slab region

Figure 5.4: Waveguide output images

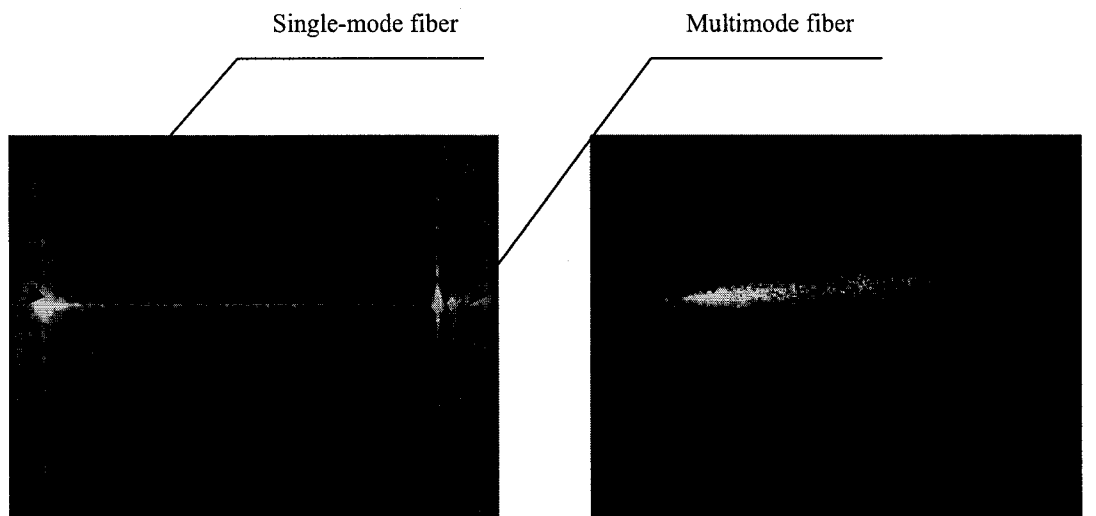
5.1.2 Analysis

As seen from the above figures, most of the light is confined under the strip in the chalcogenide glass. The mode field shape is gaussian-like except the top, which is rounded due to the saturation of the camera.

There is a discrepancy between the theoretical and measured profiles in that the predicted modes are more tightly bound than the measured modes. One possible reason for this inconsistency is that the tested waveguide sections are not long enough to let the slab modes in BCB leak away.

5.2 Evaluation of waveguide losses

5.2.1 Light propagation (top images)



a) Light propagating in waveguide region b) Light propagating in nearby slab region

Figure 5.5: Light propagating in a straight waveguide

The light scattered from the waveguides is captured using the setup shown in Figure 2.11, and the top images, which represent the light evolution inside the waveguides, are derived with the help of Studio DC10plus, a software package.

Light propagating along a straight waveguide and a splitter are shown in Figure 5.5 and Figure 5.6 respectively.

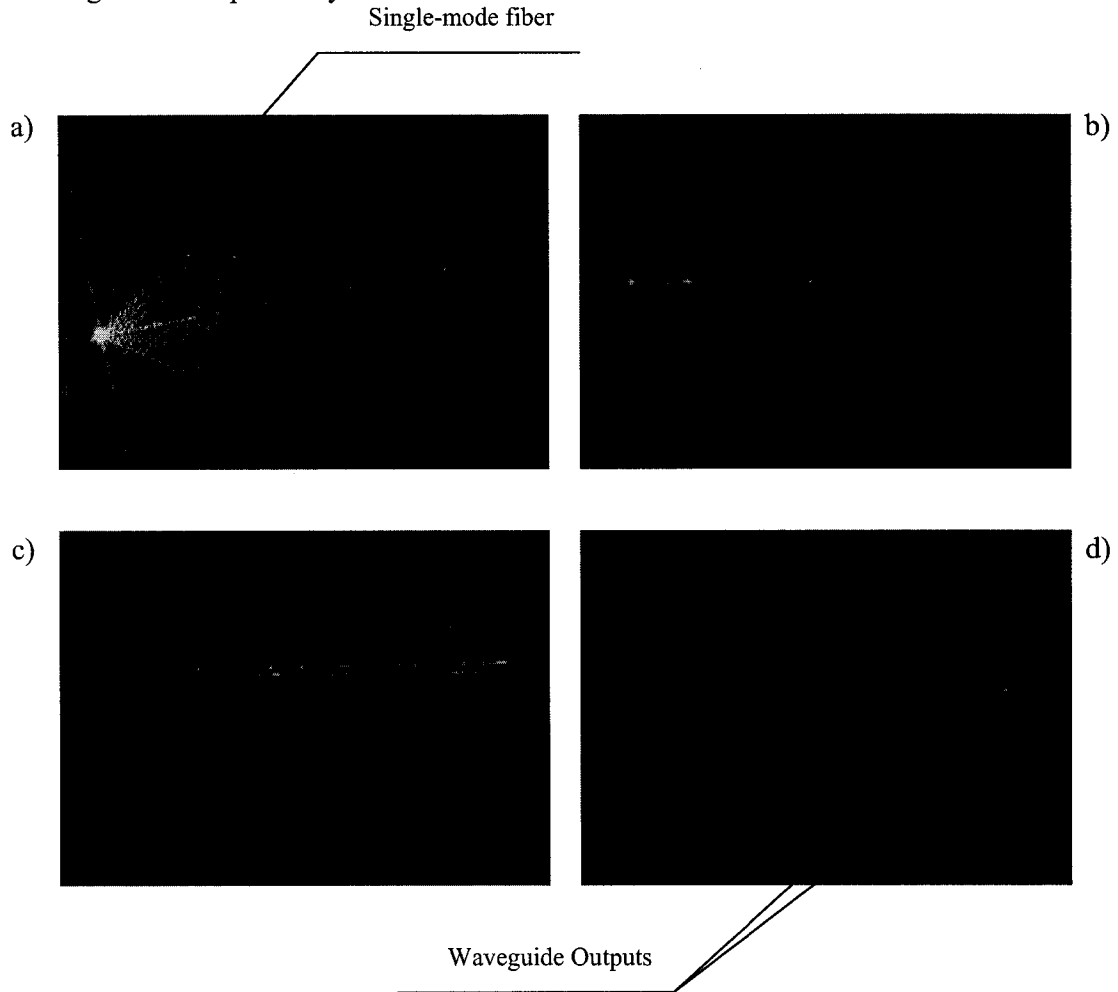


Figure 5.6: Light propagating in a Y-splitter: a) light coupling into waveguide; b) splitting; c) further splitting apart; d) light coming out.

5.2.2 Loss measurement

1) Propagation loss

As the scattered light power can be derived in terms of the propagation distance from Figure 5.5 using IPLab, the attenuation coefficient can be obtained using equation 2.4.

A plot of the logarithm of the scattered light power is shown in Figure 5.7 as a function of propagation distance. Considering a large amount of light is lost at both ends due to the mode mismatch, a straight line least squares curve fitting was carried out for the region from 1.2 mm to 6.7 mm. The slope gives the propagation loss value of around 1 dB/cm.

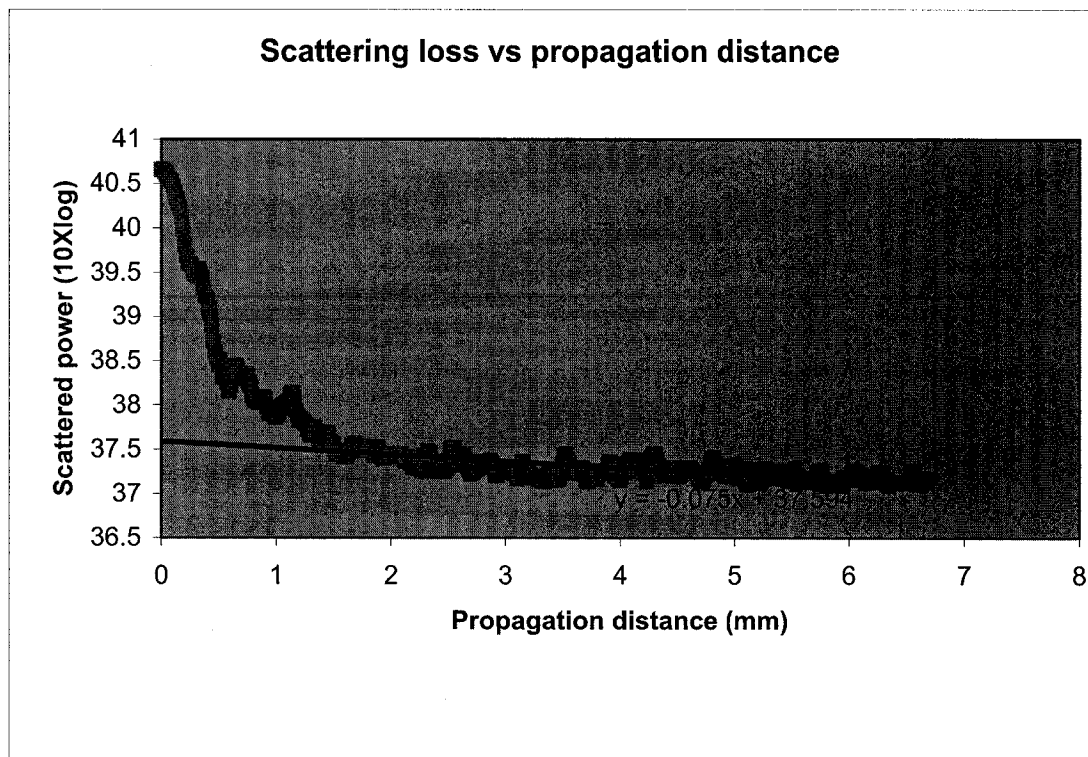


Figure 5.7: Scattering loss vs. propagation distance

2) Total loss

An 18 dB total loss, which includes propagation loss and coupling loss, is observed for a 6.7 mm long strip-loaded shallow rib waveguide. This implies that the propagation loss (including scattering loss and absorption loss) is negligible compared to the coupling loss. The coupling loss needs to be further analyzed.

5.2.3 Analysis

1) Coupling loss

The coupling loss contributes ~ 17 dB to the total loss. First of all, it is believed that the high coupling loss is due to the field mismatching [shown in Figure 5.7], which can be calculated by integrating the input field with the waveguide field.

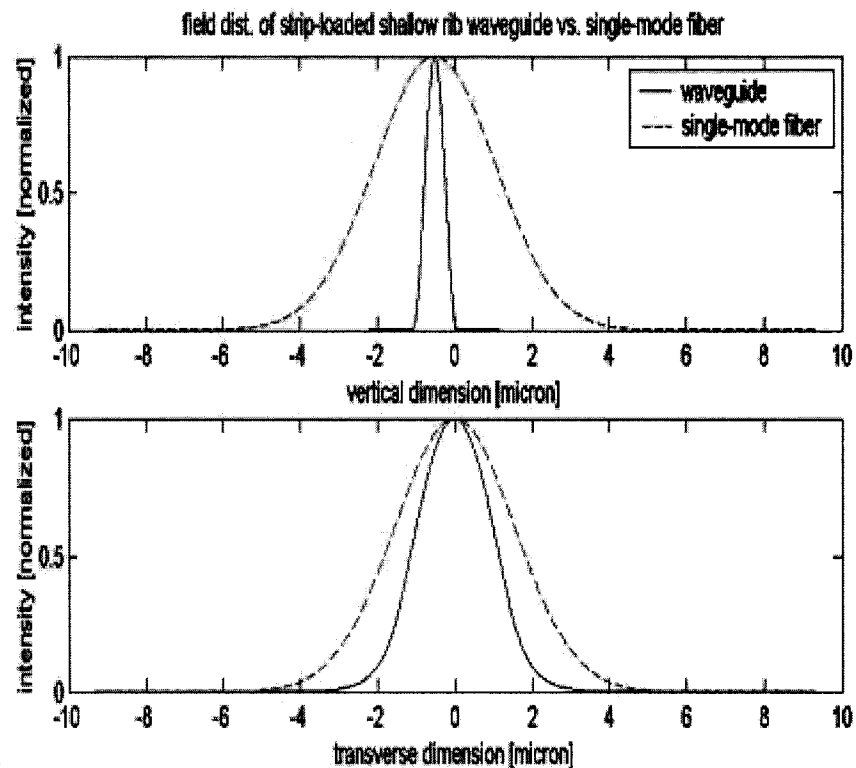


Figure 5.8: Field profiles of a fabricated waveguide and a single-mode fiber

It is found that the field mismatching loss for the case of end-coupling from a single-mode fiber ($9\ \mu\text{m}$) to a strip-loaded shallow rib waveguide (rib width: $3.8\ \mu\text{m}$) is around 7 dB (see Appendix V for Matlab code).

The remaining loss ($18\ \text{dB} - 8\ \text{dB} = 10\ \text{dB}$) is attributed to waveguide separation, misalignment and edge roughness (see Figure 5.9).

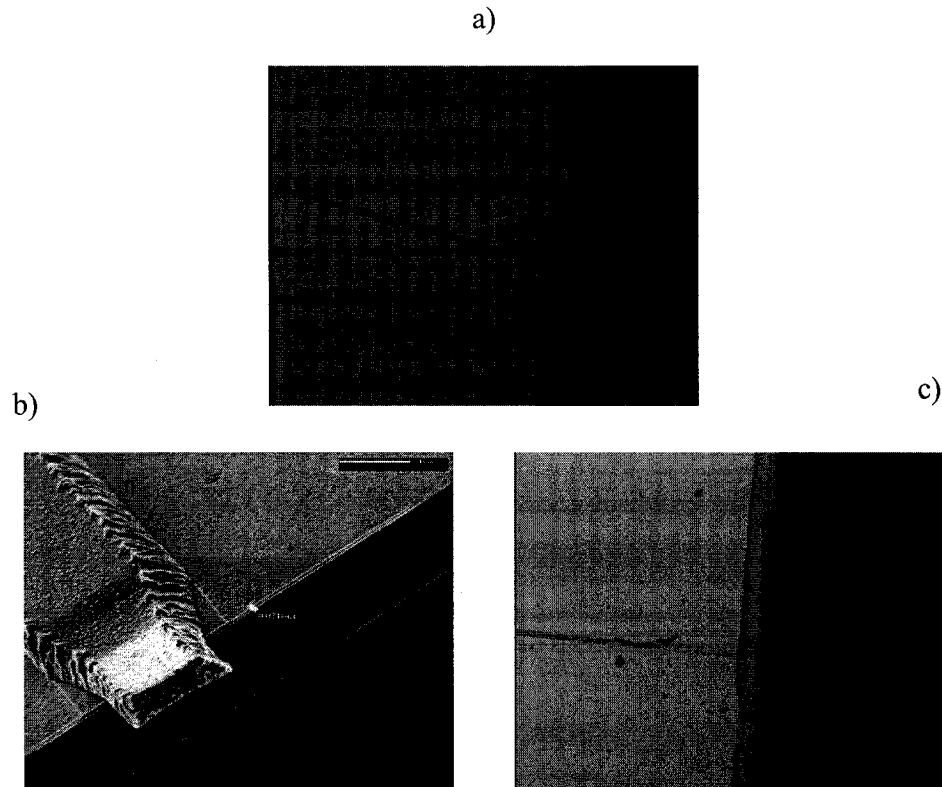


Figure 5.9: Edge roughness of the fabricated waveguides: a) Uneven cleaving; b) Strip stretching; c) Strip piling off.

A thicker As_2Se_3 layer, as well as matching gel can reduce field-mismatching loss. However, special care needs to be taken, as adhesion decreases with thickness. For loss due to edge roughness, polishing can be the help, but toxicity of As_2Se_3 is a concern.

6. Other explored CHG waveguide structures

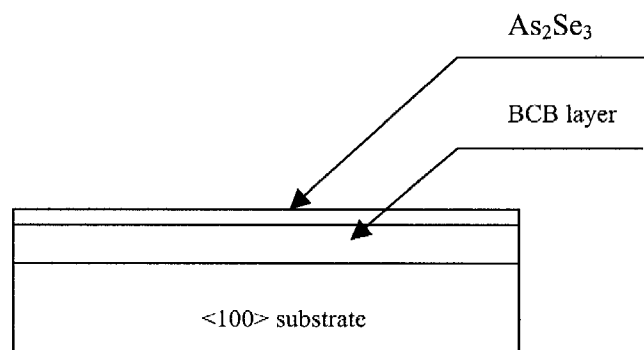
Other CHG waveguide structures were also explored in this project, including laser-written channel waveguides. Laser-written waveguides are attractive for their simplicity in fabrication.

Chalcogenide glasses undergo photo-induced structural changes when exposed to near bandgap light [33]. Such changes can be optical, e.g. photo-darkening and refractive index change. Taking advantage of this property of chalcogenide glass, a variety of features can be patterned on chalcogenide thin film with suitable exposure techniques [34], thus waveguides can be made [35].

The structural change of chalcogenide thin film is wavelength and intensity dependent [36]. A 633 nm HeNe laser is applied for writing waveguides in As_2Se_3 films, as HeNe laser can change the refractive index of As_2Se_3 films up to 0.04 [37]. A typical fabrication process of laser-written CHG waveguides normally involves the following steps:

1. Chalcogenide thin film preparation

Chalcogenide films are prepared as in strip-loaded shallow rib waveguides.



2. Laser-writing

The laser-writing setup is shown in Figure 6.1. Mirrors and lens are used to direct and focus the laser beam onto As_2Se_3 films, while computerized moving stage controls the exposed spot and exposure duration.

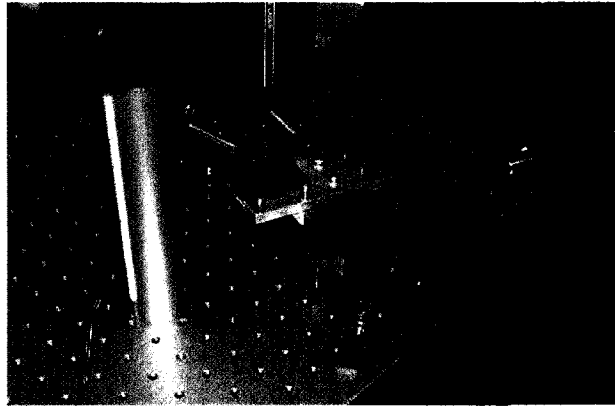


Figure 6.1: Laser-writing setup

The fabricated laser-written waveguides are as shown in Figure 6.2. Due to time constraints, these laser-written waveguides have not been tested, and there are still several unknowns, such as index profile of As_2Se_3 films after exposure. It is generally believed that light confinement in these waveguides is weaker than in rib waveguides.

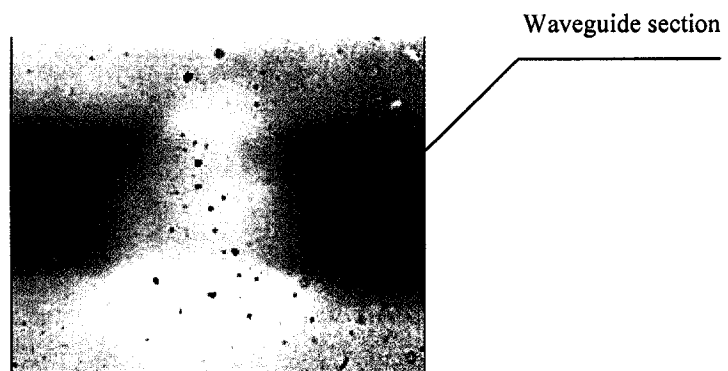


Figure 6.2: Microscope picture showing a laser-written waveguide (dark strip)

7. Conclusions

7.1 Summary of work

In this project, chalcogenide glass, As_2Se_3 , was investigated. State-of-the-art rib waveguides, as well as strip-loaded shallow rib waveguides have been designed and simulated using the effective index method, the finite difference method and the beam propagation method.

The waveguides were fabricated using standard micro-fabrication techniques. While the inverted rib waveguides could not be fabricated as proposed due to the adhesion and the step coverage problem of As_2Se_3 films, the strip-loaded shallow rib waveguides were feasible. The shape and the dimension of the fabricated strip-loaded shallow rib waveguides are generally as expected.

The fabricated strip-loaded shallow rib waveguides were tested using the scattering loss and the near-field profile measurement. The waveguides exhibited a low propagation loss (~ 1 dB/cm at wavelength of 980 nm). However, the coupling losses (from a 9 μm single-mode fiber to these waveguides) are very high (~ 17 dB) due to the mode mismatch, which eventually results in a very high total loss (~ 18 dB for a 6.7 mm long CHG strip-loaded shallow rib waveguide).

7.2 Suggestions for future work

The first appropriate step towards the feasibility of waveguides in As_2Se_3 would be implementing a consistent and reliable etching solution. This can be done by either further improving the adhesion of As_2Se_3 films or developing a technique to etch As_2Se_3 without substantially degrading the films.

Other potentials that can be looked into for a better waveguide in As_2Se_3 include using photo-induced dissolution rate change of chalcogenide glasses [38] in making

waveguides, applying thicker core layer and different strip material for strip-loaded shallow rib waveguides.

Bibliography

1. Miller, S.E., "Integrated optics: an introduction", *The Bell System Technical Journal*, Vol.48, No.7, pp. 2059-2069, Sep. 1969.
2. Hiroshi Nishihara, Masamitsu Haruna, Toshiaki Suhara, *Optical Integrated Circuits*, NY: McGraw-Hill Book Company, pp.2, 1987.
3. Kolobov, V. Alexander and Kazunobu Tanaka, *Photoinduced Phenomena in Amorphous Chalcogenides: From Phenomenology to Nanoscale, Handbook of Advanced Electronic and Photonic Materials and Devices*. San Diego, CA: Academic Press, 2001.
4. Jon Petursson, J. M. Marshall, A.E. Owen, "Optical absorption in As-Se glasses", *Philosophical Magazine B*, Vol. 63, No. 1, pp.15-31, 1991.
5. Viens, Jean-Francois, Chiara Meneghini, Tigran V. Galsian, K.A. Richardson and T. Cardinal, "Fabrication and Characterization of Integrated Optical Waveguides in Chalcogenide Glasses", *Journal of Lightwave Technology*, Vol. 17, No. 7, pp. 1184-1191, July 1999.
6. M.S. Sodha and A.K. Ghatak, *Inhomogeneous Optical Waveguides*, New York: Plenum Press, 1977.
7. Lynn D. Hutcheson, *Integrated Optical Circuits and Components*, New York and Basel: Marcel Dekker, Inc., 1987.
8. Andrea Melloni, Paolo Monguzzi, Raffaella Costa and Mario Martinelli, "Design of curved waveguides: the matched bend", *Optical Society of America*, Vol. 20, No. 1, pp.130-137, January 2003.
9. W. J. Minford, S. K. Korotky, and R.C. Alfarness, "Low-loss Ti:LiNbO₃ waveguide bends at $\lambda=1.3 \mu\text{m}$ ", *Quantum Electronics*, QE-18, pp.1802, 1982.
10. Clifford R. Pollock, *Fundamentals of Optoelectronics*, Chicago: Richard D. Irwin, Inc., pp. 299, 1995.

11. William B. Jones, Jr., *Introduction to Optical Fiber Communication Systems*, NY: Holt, Rinehart and Winston, Inc., pp.34-80, 1987.
12. M. J. Adams, *An Introduction to Optical Waveguides*, New York: Wiley Press, 1981.
13. Joseph T. Boyd, *Integrated Optics Devices and Applications*, NY: The Institute of Electrical and Electronics Engineers, Inc., 1990.
14. S. Iraj Najafi, *Introduction to glass integrated optics*, Boston: Artech House, Inc. 1992.
15. Rsoft Design Group, Inc., *BeamPROP Version 5.0c*, New York: Columbia University, 1993.
16. Marc Madou, *Fundamentals of Micro-fabrication*, Boca Raton: CRC Press LLC, 1997.
17. Plummer Deal, *Silicon VSDL Technology*, NJ: Prentice Hall, 2000.
18. Richard C. Jaeger, *Introduction to Microelectronic Fabrication*, MA: Addison-Wesley Publishing Company, Inc., 1993.
19. E. A. J. Marcatili, "Slab-Coupled waveguides", *The Bell System Technical Journal*, Vol. 53, No. 4, pp. 645-675, April 1974.
20. Souren P. Pogossian, Lili Vescan, Adrian Vonsovici, "The Single-Mode Condition for Semiconductor Rib Waveguides with Large Cross Section", *Journal of Lightwave Technology*, Vol. 16, No. 10, pp. 1851-1853, Oct. 1998.
21. Richard A. Soref, Joachim Schmidchen, Klaus Petermann, "Large Single-mode Rib Waveguides in GeSi-Si and Si-on-SiO₂", *Journal of Quantum Electronics*, Vol. 27, No. 8, pp. 1971-1974, August 1991.

22. Song-Tusen Peng, Arthur A. Oliner, "Guidance and Leakage Properties of a Class of Open Dielectric Waveguide: Part I-Mathematical Formulations", *Transactions on Microwave Theory and Techiques*, Vol. MTT 29, No. 9, pp. 843-855, Sep. 1981.
23. Song-Tusen Peng, Arthur A. Oliner, "Guidance and Leakage Properties of a Class of Open Dielectric Waveguide: Part II-New Physical Effects", *Transactions on Microwave Theory and Techiques*, Vol. MTT 29, No. 9, pp. 855-869, Sep. 1981.
24. RAJ Mittra, Yun Li Hou, Vahraz Jamnejad, "Analysis of Open Dielectric Waveguides Using Mode-Matching Technique and Variational Methods", *Transactions on Microwave Theory and Techniques*, Vol. MTT-28, No. 1, pp. 36-43, January 1980.
25. Ulrich Crombach, "Analysis of Single and Coupled Rectangular Dielectric Waveguides", *Transactions on Microwave Theory and Techniques*, Vol. MTT-29, No. 9, pp. 870-874, Sept. 1981.
26. K. Petermann, "Properties of Optical Rib-guides with Large Cross-section", *Archiv fur Elektronik und Ubertragungstechnik*, (Germany), Vol. 30, pp. 139-140, 1976.
27. Nadir Dagli, Clifton G. Fonstad, "Anaysis of Rib Dielectric Waveguides", *Journal of Quantum Electronics*, Vol. QE-21, No. 4, pp. 315-321, April 1985.
28. G. Fischbeck, R. Moosburger, M. Topper and K. Petermann, "Design concept for single mode polymer waveguides", *Electronics Letters*, Vol. 32, No. 3, pp. 212-213, Feb. 1996.
29. R. Moosburger, K. Petermann, "4X4 Digital Optical Matrix Switch Using Polymeric Oversized Rib Waveguides", *Photonics Technology Letters*, Vol. 10, No. 5, pp. 684-686, May 1998.
30. A. G Rickman, G.T. Reed, Fereydoon Namavar, "Silicon-on-Insulator Optical Rib Waveguide Loss and Mode Characteristics", *Journal of Lightwave Technology*, Vol. 12, No. 10, pp. 1771-1776, Oct. 1994

31. M. Krishnaswamy, J. N. McMullin, B.P. Keyworth, J. S. Hayden, "Optical properties of strip-loaded Er-doped waveguides", *Optical Materials*, pp. 287-292, Nov. 1996.
32. V. Ramaswamy, "Strip-loaded Film Waveguide", *The Bell System Technical Journal*, Vol. 53, No. 4, pp. 697-703, April 1974.
33. Keiji Tanaka, "Photoinduced Structural Changes in Chalcogenide Glasses", *Reviews of Solid State Science*, Vol. 4, No. 2&3, pp. 641-659, 1990.
34. A. Zakery, P.J. S. Ewen, A. E. Owen, "Photodarkening in As-S films and its application in grating fabrication", *Journal of Non-Crystalline Solids*, pp. 768-773, 198-200 (1996).
35. Arshad K. Mairaj, Ping Hua, Harvey N. Rutt, Daniel W. Hewak, "Fabrication and Characterization of Continuous Wave Direct UV ($\lambda=244\text{nm}$) Written Channel Waveguides in Chalcogenide (Ga:La:S) Glass", *Journal of Lightwave Technology*, Vol. 20, No. 8, pp. 1578-1584, August 2002.
36. Madan, Arun and Melvin P. Chaw, *The Physics and Application of Amorphous Semiconductors*, San Diego: Academic Press, pp. 318-351, 1998.
37. A. C. van Popta, R. G. DeCorby, C. J. Haugen, T. Robinson, and J. N. McMullin, D. Tonchev and S. O. Kasap, "Photoinduced refractive index change in As_2Se_3 by 633nm illumination", *Optics Express*, Vol. 10, No. 15, pp. 639-644, 2002.
38. Anisimova, N. I., G.A. Bordovsky, V.A. Bordovsky and R.A. Castro, "The Photoinduced Change of Dissolution Rate In As_2Se_3 Glasses", *Radiation Effect & Defects in Solids*, Vol. 156, pp. 365-369, 2001.

Appendix I: Summary of EI method

In the EI method, the transverse field is decoupled in X and Y direction and is assumed to be transverse electrical field (TE) or transverse magnetic field (TM). Thus the effective index, the index seen by the mode, of the structure is obtained by successively solving two transcendental slab equations.

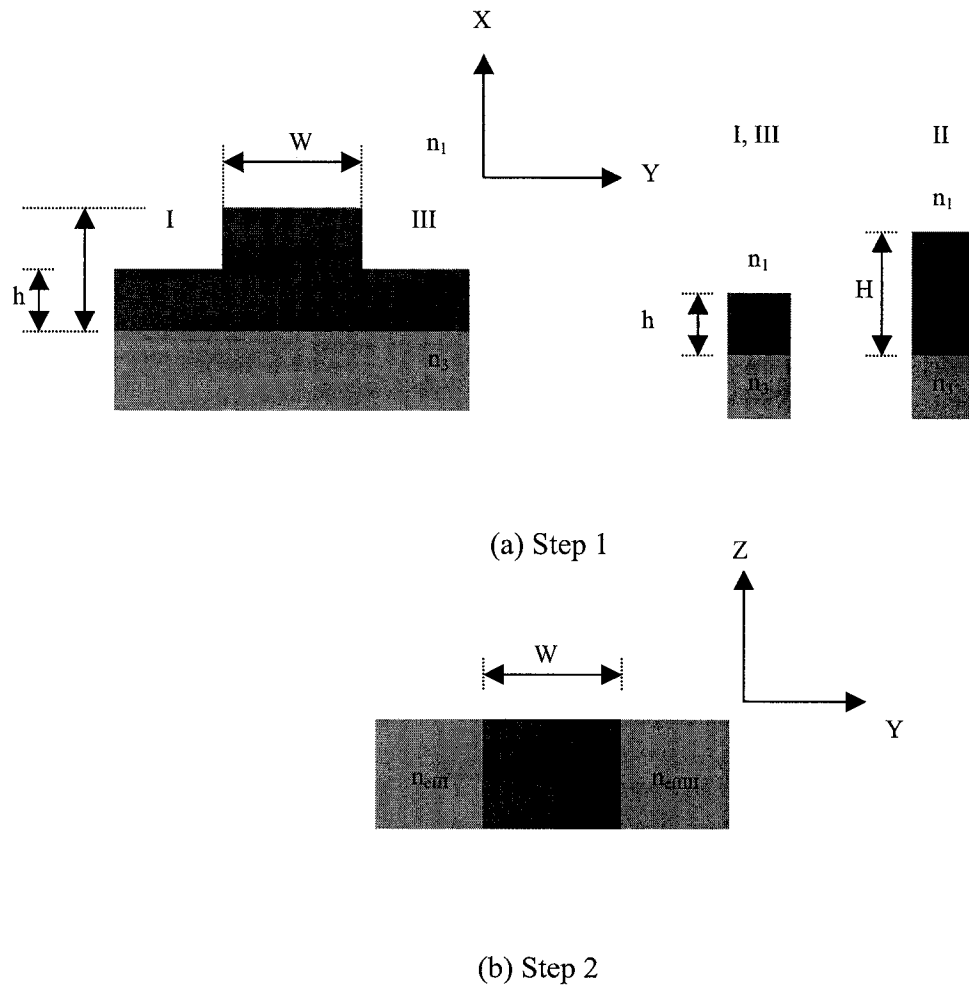


Figure A1: Effective index method approach

In the case of a rib waveguide, the method in the first step solves transcendental equations for three vertical slabs [Figure A1 (a)]. The effective indices can be obtained by the standard TE eigenvalue equation for asymmetric slab waveguide:

$$\tan(ht) = \frac{p + q}{h(1 - \frac{pq}{h^2})} \quad (3.8)$$

where: $h = [(n_2 k_0)^2 - \beta^2]^{1/2}$; $q = [\beta^2 - (n_1 k_0)^2]^{1/2}$; $p = [\beta^2 - (n_3 k_0)^2]^{1/2}$,

β is mode propagation constant,

$$n_{eff} = \frac{\beta}{K_0}, \quad n_{eff} = \frac{\beta \lambda_0}{2\pi}, \quad \lambda_0 \text{ is free space wavelength.}$$

And the three derived effective indices are used as the refractive indices for a horizontal slab waveguide as shown in Figure A1 (b). The effective index of the original rib waveguide is approximated by solving the TM eigenvalue equation for the horizontal symmetric slab waveguide [20]:

$$\tan(ht) = \frac{h(\bar{p} + \bar{q})}{h^2 - \bar{p}\bar{q}} \quad (3.9)$$

where: $\bar{p} = \frac{n_2^2}{n_3^2} p$; $\bar{q} = \frac{n_2^2}{n_1^2} q$.

Appendix II

```
% This m-file codes the single mode condition for rib waveguides with large cross
section
% base on 1) effective index method  $t < r/(1-r^2)^{0.5}$ 
%      2) beam propagation method  $r < 0.5$ 
%
%  $h\_H$ =height of the core material outside the rib/height of the rib in the core section
%
% Required input variable:
% H=height of the rib in the core section
% ncore=refractive index of the core material
ncore=2.5;
% nup=refractive index of the upper cladding
nup=1;
% ndown=refractive index of the lower cladding
ndown=1.45;
% lambda=free-space wavelength
lambda=1550e-9;
%
k0=2*pi/lambda;
h_H=0.5:0.01:0.8;
H=h./h_H;
%
% for TE mode
garmac=1;
garmas=1;
%
q=garmac/(k0*(ncore^2-nup^2))+garmas/(k0*(ncore^2-ndown^2));
Heff=H+q;
heff=h+q;
r=heff./Heff;
%
if r>0.5
    t=r./(1-r.^2).^0.5;
end
Weff=t.*Heff;
w=Weff-2*garmac/(k0*(ncore^2-nup^2))
%
% Generate plots
%
plot(w*1e6,H*1e6)
xlabel('the width of the rib')
```

ylabel('the high of the rib')

Appendix III

```
% This following m-file codes the single mode condition for strip-loaded shallow rib
waveguide
% base on 1) mode matching technique
%      2) beam propagation method  $r > 0.5$ 
%
clc
clear
% r=height of the core material outside the rib/height of the rib in the core section
%
% H=height of the rib in the core section(um)
H=1e-6;
% ncore=refractive index of the core material
ncore=2.72;
% nup=refractive index of the upper cladding
nup=1;
% ndown=refractive index of the lower cladding
ndown=1.62;
% nstrip=refractive index of the strip
nstrip=1.56;
% w=the width of the strip
%
% lambda=free-space wavelength
lambda=1550e-9;
%
% for TE mode
garmac=1;
garmas=1;
%
k0=2*pi/lambda;
r=0.5:0.01:1;
b=H/(2*lambda);
qout=garmac/sqrt(ncore^2-nup^2)+garmas/sqrt(ncore^2-ndown^2);
qin=garmac/sqrt(ncore^2-nstrip^2)+garmas/sqrt(ncore^2-ndown^2);
%
w1=4*pi*b/(qin+4*pi*b);
w2=4*pi*b*r/(qout+4*pi*b*r);
delta=(w2./(r*w1)).^2-1;
a=b*(0.3+1./sqrt(delta))/w1;
w=2*a*lambda;
%
% Generate plots
%
plot(w*1e6,H*r*1e6)
```

```

ylabel('the height of the outside(um)')
xlabel('the width of the rib(um)')
hold on
%
%
% This following m-file codes the single mode condition for rib waveguides with large
cross section
% base on 1) effective index method  $t < r/(1-r^2)^{0.5}$ 
% 2) beam propagation method  $r < 0.5$ 
%
%
h=H*r;
%
% for TE mode
garmac=1;
garmas=1;
%
q=garmac/(k0*(ncore^2-nup^2))+garmas/(k0*(ncore^2-ndown^2));
Heff=H+q;
heff=h+q;
reff=heff./Heff;
%
if reff>0.5
    t=reff./(1-reff.^2).^0.5;
end
Weff=t.*Heff;
w=Weff-2*garmac/(k0*(ncore^2-nup^2))
%
% Generate plots
%
plot(w*1e6,h*1e6,'r--')
title('The height of the side region vs the width of the rib for H=1 um')
legend('strip-loaded rib waveguide','rib waveguide')
gtext('single-mode region')
gtext('multi-mode region')
%
```

Appendix IV

```
% This Matlab program is modified from Dr. Decorby's program.
% This program codes the effective index method for analyzing
% strip-loaded shallow rib waveguide.
% The guide is assumed to be single-moded, and the fundamental TE mode is
% solved. The guide is assumed to have different material for upper and lower claddings.
% The outputs are the effective modal index.
%
clc
clear
% REQUIRED INPUT VARIABLES:
% w=the width of the rib
w=3.0e-006:0.1e-006:3.0e-006;
% H=height of the rib in the core section
H=1.0e-006;
% h=height of the core material outside the rib
%
% ncore=refractive index of the core material
ncore=2.72;
% nstrip=refractive index of the strip material
nstrip=1.54;
% nup=refractive index of the upper cladding
nup=1;
% ndown=refractive index of the lower cladding
ndown=1.62;
% lambda=free-space wavelength
lambda=1550e-009;
%
k0=2*pi/lambda;
%
% calculate the maximum value of transverse wave vector in core, based on total
% internal reflection:
kapmax=sqrt(k0^2*(ncore^2-ndown^2));
%
% calculate starting guesses for transverse propagation vectors, based on
% the one-half-wavelength between reflecting boundaries condition:
kaprib0=pi/(2*H); % starting guess in 'region II'
if kaprib0>kapmax
    kaprib0=kapmax;
end
%
% solve numerically for the propagation vectors of fundamental modes
%
% split along y into regions I,II,III, solve as asymmetric slabs confined along x:
```

```

% region I (the rib):
kaprib=fminsearch('eigenasymm',kaprib0,[],H,k0,ncore,nstrip,ndown);
Neffrib=sqrt(k0^2*ncore^2-kaprib^2)/k0
%
kaptran0=pi./(2*w);
%
% for TE mode
garmac=1;
garmas=1;
%
k0=2*pi/lambda;
b=H/(2*lambda);
qout=garmac/sqrt(ncore^2-nup^2)+garmas/sqrt(ncore^2-ndown^2);
qin=garmac/sqrt(ncore^2-nstrip^2)+garmas/sqrt(ncore^2-ndown^2);
%
w1=4*pi*b/(qin+4*pi*b);
%
for n=1:1:1
a=w(n)/(2*lambda);
%
r=0.8:0.002:1
w2=4*pi*b*r./(qout+4*pi*b*r);
delta=(w2./(r*w1)).^2-1;
for m=1:1:101
if a<(0.3+1/sqrt(delta(m)))*b/w1
h(m)=H*r(m);
% region II (outside the rib):
kapout0(m)=pi/(2*h(m));% starting guess in 'region I and III'
if kapout0(m)>kapmax
kapout0(m)=kapmax;
end
kapout(m)=fminsearch('eigenasymm',kapout0(m),[],h(m),k0,ncore,nup,ndown);
Neffout(m)=sqrt(k0^2*ncore^2-kapout(m)^2)/k0
%
% Analyze transverse confinement by viewing the rib from the top view as a symmetric
% slab confined along the y-direction with cladding index Neffout and core index Neffrib
% (note that we should solve a TM eigenvalue equation here, since the electric field is
% assumed to be primarily along y in the plane of the substrate):
%
kaptran(m)=fminsearch('eigensymmTM',kaptran0(n),[],w(n),k0,Neffrib,Neffout(m));
Neff(m)=sqrt(k0^2*Neffrib^2-kaptran(m)^2)/k0; %overall effective index for the
fundamental TE mode.
%
subplot(4,2,n)
plot((H-h(m))*1e6, Neffrib,'kx',(H-h(m))*1e6, Neffout(m),'ko',(H-h(m))*1e6,
Neff(m),'k^')

```

```
xlabel('Etching depth [micron]')
ylabel('Effective index')
title(['H=1um, w=',num2str(w(n))])
legend('effective index of the rib region','effective index outside of the rib','effective
modal index')
hold on
end
end
end
```

Appendix V

```
%Matlab code for calculating the coupling coefficient from fiber to strip-loaded shallow
rib waveguides
%
%The following m-file codes the Gaussian field profile of single-mode fibre
%
clc
clear
% lambda=free-space wavelength
lambda=980e-009;
%
k0=2*pi/lambda;
% core refractive index n1
n1=1.5362;
% cladding refractive index n2
n2=1.5306;
% core diameter a
a=5.5e-006/2;
% vacuum impedance z0
z0=377;
% normalized frequency V
V=a*k0*sqrt(n1^2-n2^2);
% mode spot radius w0
w0=a*(0.65+1.619*V^(-1.5)+2.879*V^(-6));
%
% This following m-file codes the effective index method for analyzing a strip-loaded
shallow rib waveguide.
% The guide is assumed to be single-moded, and the fundamental TE mode is
% solved. The guide is assumed to have different material for upper and lower claddings.
% The outputs are the effective modal index and the approximate field profile.
% The file calls eigenasymm.m and eigensymmTM.m, which are function files that code
the
% eigenvalue equations for TE and TM propagation in asymmetric and symmetric slab
% waveguides, respectively.
%
% REQUIRED INPUT VARIABLES:
% w=the width of the rib
w=3e-006;
% H=height of the rib in the core section
H=1e-006;
% h=height of the core material outside the rib
h=0.9e-006;
% ncore=refractive index of the core material
ncore=2.72;
```

```

% nstrip=refractive index of the strip material
nstrip=1.54;
% nup=refractive index of the upper cladding
nup=1;
% ndown=refractive index of the lower cladding
ndown=1.62;
%
% calculate the maximum value of transverse wave vector in core, based on total
% internal reflection:
kapmax=sqrt(k0^2*(ncore^2-ndown^2));
%
% calculate starting guesses for transverse propagation vectors, based on
% the one-half-wavelength between reflecting boundaries condition:
kaprib0=pi/(2*H); % starting guess in 'region II'
kapout0=pi/(2*h); % starting guess in 'region I and III'
if kaprib0>kapmax
kaprib0=kapmax;
end
if kapout0>kapmax
kapout0=kapmax;
end
%
% solve numerically for the propagation vectors of fundamental modes
%
% split along y into regions I,II,III, solve as asymmetric slabs confined along x:
% region I (the rib):
kaprib=fminsearch('eigenasymm',kaprib0,[],H,k0,ncore,nstrip,ndown);
betarib=sqrt(k0^2*ncore^2-kaprib^2);
gammribup=sqrt(k0^2*(ncore^2-nstrip^2)-kaprib^2);
gammribdown=sqrt(k0^2*(ncore^2-ndown^2)-kaprib^2);
Neffrib=betarib/k0
%
% region II (outside the rib):
kapout=fminsearch('eigenasymm',kapout0,[],h,k0,ncore,nup,ndown);
betaout=sqrt(k0^2*ncore^2-kapout^2);
gammoutup=sqrt(k0^2*(ncore^2-nup^2)-kapout^2);
gammoutdown=sqrt(k0^2*(ncore^2-ndown^2)-kapout^2);
Neffout=betaout/k0
%
% Analyze transverse confinement by viewing the rib from the top view as a symmetric
% slab confined along the y-direction with cladding index Neffout and core index Neffrib
% (note that we should solve a TM eigenvalue equation here, since the electric field is
% assumed to be primarily along y in the plane of the substrate):
%
kaptran0=pi/(2*w);
%

```

```

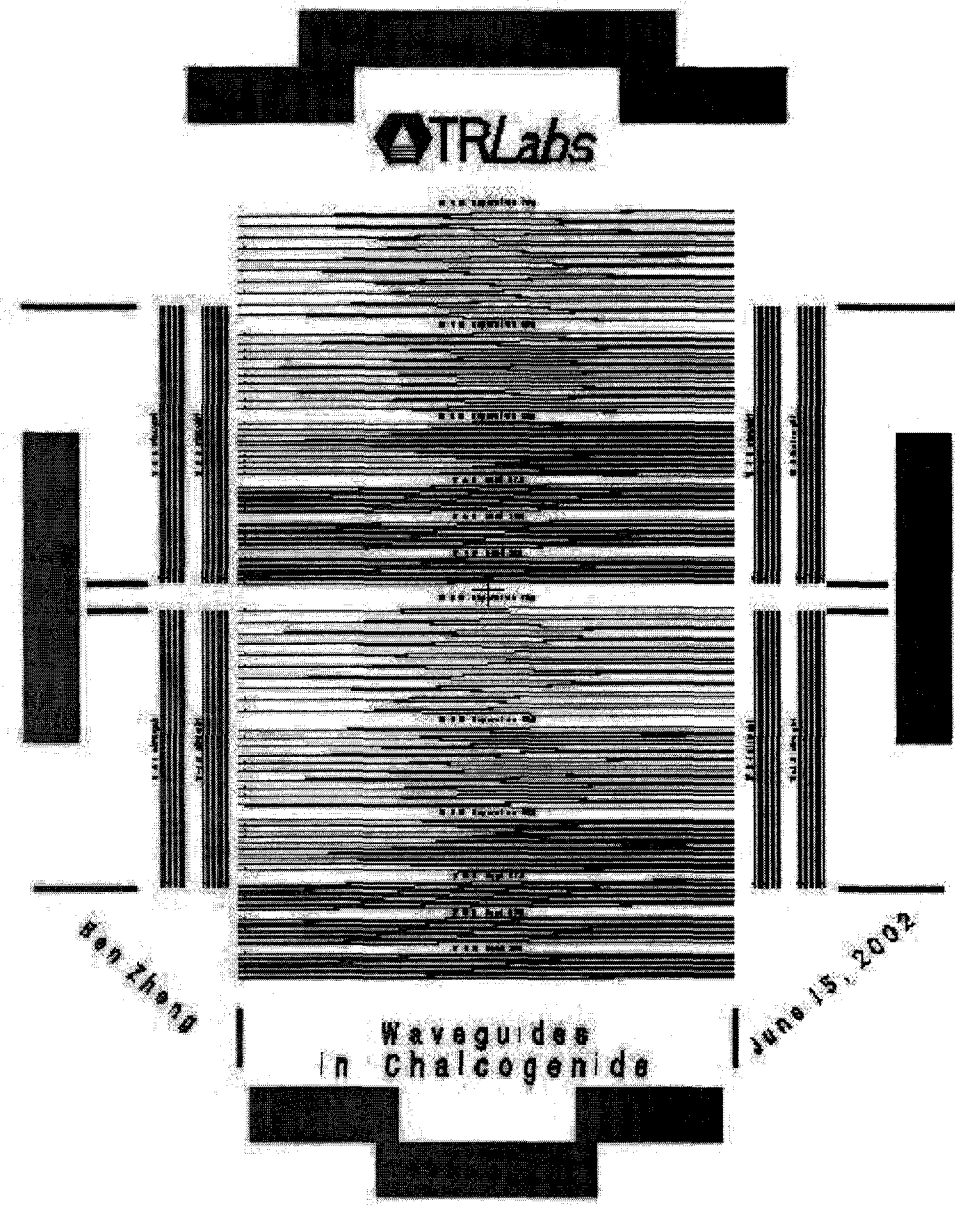
kaptran=fminsearch('eigensymmTM',kaptran0,[],w,k0,Neffrib,Neffout);
betatran=sqrt(k0^2*Neffrib^2-kaptran^2);
gammtran=sqrt(k0^2*(Neffrib^2-Neffout^2)-kaptran^2);
Neff=betatran/k0 %overall effective index for the fundamental TE mode.
%
% field distributions for the strip-loaded shallow rib waveguide
%
% create coordinate vector in x, with origin at top of the rib:
X=-3*w0:0.01*H:3*w0;
Xm=X*1e6; % x-coordinate in microns
% create coordinate vector in y, with origin in the centre of the rib:
Y=-3*w0:0.01*w:3*w0;
Ym=Y*1e6; % y-coordinate in microns
%
% approximate the x-dependence of the field using the eigenvalues from the asymmetric
% slab solution INSIDE the rib above:
for q=1:length(X)
fieldx_r(q)=asymmslabfield(H,kaprib,gammribup,gammribdown,X(q));
end
% approximate the y-dependence of the field using the eigenvalues from the symmetric
% slab solution above:
for qq=1:length(Y)
fieldy_r(qq)=symmslabfield(w,kaptran,gammtran,Y(qq));
end
%
% Calculate the transverse intensity profiles (normalized):
%
intensx_r=fieldx_r.^2;
intensity_r=fieldy_r.^2;
intensxN_r=intensx_r/max(intensx_r);
intensityN_r=intensity_r/max(intensity_r);
%
% field distributions for the 980nm single-mode fiber
%
% approximate the x and dependence of the field using the Gaussian approximation
for q=1:length(X)
fieldx_f(q)=2*sqrt(n2/(z0*pi))*exp(-((X(q)+H/2)/w0)^2)/w0;
end
for qq=1:length(Y)
fieldy_f(qq)=2*sqrt(n2/(z0*pi))*exp(-(Y(qq)/w0)^2)/w0;
end
%
% Calculate the transverse intensity profiles (normalized):
%
intensx_f=fieldx_f.^2;
intensity_f=fieldy_f.^2;

```

```

intensxN_f=intensx_f/max(intensx_f);
intensityN_f=intensity_f/max(intensity_f);
%
% Generate plots
%
subplot(3,1,1)
plot(Xm,intensxN_r,Xm, intensxN_f,'r--')
xlabel('vertical dimension [micron]')
ylabel('intensity [normalized]')
title('field dist. of strip-loaded shallow rib waveguide vs. single-mode fiber')
legend('waveguide','single-mode fiber')
subplot(3,1,2)
plot(Ym,intensityN_r,Ym, intensityN_f,'r--')
xlabel('transverse dimension [micron]')
ylabel('intensity [normalized]')
%
```

Appendix VI



Mask layout

Appendix VII

1. Photolithography recipe

➤ Coating:

- Positive photoresist (HPR 504)
- Turn on spinner
- Turn on AB-M mask aligner (after turn on, press “START” button and press it down until the current is on... should hear a little beep)
- Turn on power for oven and set at 115°C for 90s
- Set the AB-M mask aligner for 4s
- On the spinner, press start and turn the “SPREAD” knob to set the speed of 500rpm. The reading should show 0.5 since it is in the unit of krpm. Set the time for 10s. The + and – buttons allow you to increase or decrease time.
- Turn the “SPIN” knob to set the speed of 4000rpm. The reading should be 4.0krpm. Set the spin time for 40s.
- Use clean room papers and spread them out on spinner table
- Place in the chuck, then put the wafer on the top of the chuck (try to make it center), and turn on the vacuum.
- Pour out some photoresist into a small beaker (clean the mouth of the bottle with clean room paper and close lid)
- Hold the beaker of photoresist with your right hand and pour down the photoresist into the center of the wafer while the left hand press the “START” button
- After finished spinning, if the resist didn’t spread out well, strip it off with acetone and start again.
- If the resist spread out nicely, then turn off the vacuum
- Carry the wafer and place it in the oven, check to see if it lies straight. Close the lid and press “START” button to bake for 90s at 115°. The Hg should be at 15.
- When hear a loud beep, press “START” button again to stop, remove the wafer and let it cool down for a few minutes.

➤ Mask Aligning:

- Turn the chuck motion down
- Place the substrate (try to make it center)
- Turn on the substrate vacuum (sub. vac.)
- Put on the mask and close the lid
- Turn on the mask vacuum

- Turn the chuck motion up and use the up/down or left/right or theta knots to make the wafer align with the mask the way you want it to be.
- Hold self-leveling and turn the knot until you feel the knot keeps slipping
- Turn on the contact vacuum and turn off the sub. vac.
- Turn the light source to expose, face away (only look when wearing a black goggles)
- When finished exposing, turn the light source back to home
- Turn off the contact vacuum and turn on the sub. vac.
- Turn the chuck motion down, if the wafer stick to the mask; turn on the nitrogen to help them separate.
- Raise the mask frame
- Turn off the sub. vac. and remove the wafer.

➤ **Developing**

- Pour out some developer 354 solution into the tray
- Place the wafer into the solution for ~15-20s
- Remove the wafer and rinse the substrate with DI water and blow dry with nitrogen gun.

➤ **Inspection**

- Place the wafer under the microscope to inspect; make sure all the features are nice and clear
- If the result is not good, strip off everything with acetone and repeat the whole procedure again.
- When done with litho, remove the mask and turn off all the powers.

➤ **Cleaning**

- Excess photoresist is poured into the photoresist waste bottle together with acetone.

Positive Photoresist

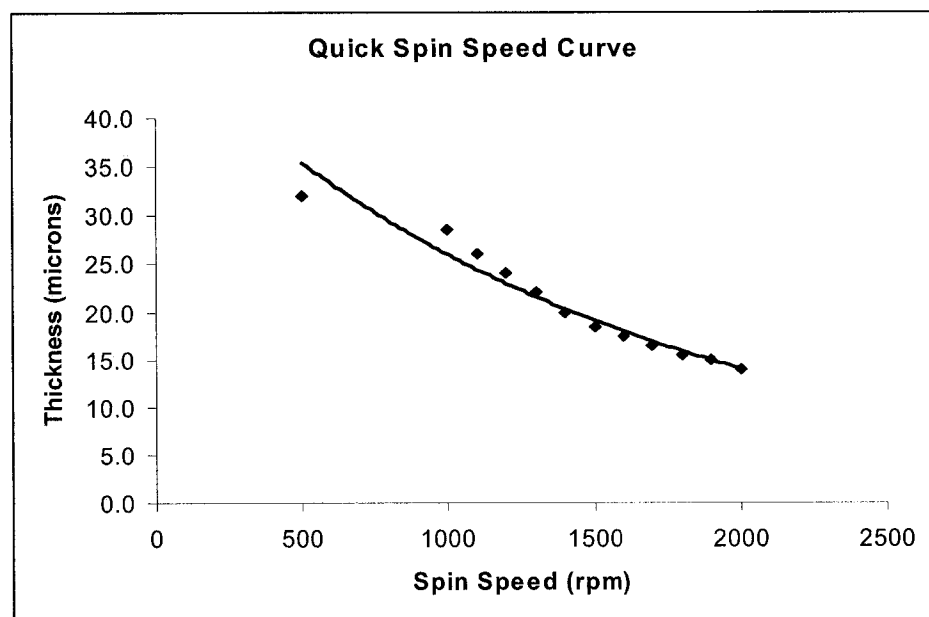
- ◆ Dark on the mask = photoresist remains
- ◆ Dark on the mask = thin film remains
 - ◆ HPR 504
 1. Spread @ 500rpm for 10s
 2. Spin @4000rpm for 40s
 3. Soft bake @115°C for 90s
 4. Expose for 4s
 5. Developer 354 for ~15-20s

6. Thickness = 1-2 microns

◆ SJR5740

1. Spread @ 200rpm for 10s
2. Spin @1500rpm for 15s
3. Let it sit in air for 5 minutes so that resist can spread out uniformly
4. Soft bake @ 105°C for 6 minutes (don't close the lid = no vacuum because the layer is too thick which may cause bubbles)
5. Expose for 18s
6. Developer 354 for 8 minutes; agitate after 5 minutes
7. Thickness = 16 microns

Note: changing the spin speed will lead to change the thickness of resist layer.



Negative Photoresist

- ◆ **Dark on the mask = photoresist gone**
- ◆ Dark on the mask = thin film removed
- ◆ AZ5214
- ◆ Developer MF321
 1. Spread @ 500rpm for 10s
 2. Spin @ 4000rpm for 40s
 3. Let it sit in air for ~2-3 minutes
 4. Vacuum bake @115°C for 90s with 5s N₂ purge
 5. Let it cool down for a few minutes
 6. Expose **with mask** for 1s

7. Bake for 3 minutes @115°C with 5s N₂ purge
8. Expose **without** mask for 20s
9. Develop for ~20s to 1 minutes

2. BCB Spinning recipe

1. After cleaning and dehydrating, the substrate is coated with Dow adhesion promoter AP3000 (Spin for 30s).
2. ~20ml of BCB is then poured into a 50ml beaker and dispensed directly on the wafer at ~100rpm using Solitec spinner until the entire wafer is coated (BCB: Dow's cyclotene 3022-63). This usually takes ~20s.
3. The polymer is then spread at 500rpm for 20s and spun at 3000rpm for 30s.
4. After spun for 30s, the spinning speed is decreased to ~400rpm and the T1100 ancillary chemical solvents (from Dow) are then added at the edge of the wafer to remove the edge bead (spin for 10s).
5. The speed is then increased to 3000rpm, and the wafer is spun for another 10s.
6. The substrate is cured in Shellab vacuum oven for one hour at 250C at last. The film is around 10 micron thick.

3. TORLON Preparation

1. TORLON comes in a fine yellow powder and must be dissolved with solution before use (60 grams of TORLON with 150mL of dimethyl formamide (DMF), mix the powder with a stir bar). The TORLON is dissolved in approximately four hours at room temperature.
2. The solution is strained using filter paper to remove any impurities. This usually takes 5hours.

4. TORLON Spinning

1. Wafers are cleaned in piranha (3:1 sulfuric acid: hydrogen peroxide) for 15 minutes first. After rinsed, the wafer is then baked at 120 C for 30 minutes to dehydrate.
2. The entire wafer is then coated with TORLON at very slow speed. Afterward the wafer is spread at 500rpm for 20s and then spun at 7000rpm for 30s.
3. The film is baked at 65 °C on hotplate for 5 minutes and another 1hr in oven at 120 °C at last. The thickness is around 1.2 microns.